A review of numerical modelling of the dynamics of microstructural development in rocks and ice: Past, present and future

S. Piazolo[1], P. D. Bons[2], A. Griera[3], M.-G. Llorens[2], E. Gomez-Rivas[4,5], D. Koehn[6], J. Wheeler[7], R. Gardner[8], J. R. A. Godinho[9,], L. Evans[8,10], R. A. Lebensohn[11,] M. W. Jessell[12]

[1] School of Earth and Environment, University of Leeds, Leeds LS2 9JT, United Kingdom

[2] Department of Geosciences, Eberhard Karls University Tübingen, Wilhelmstr. 56, 72074 Tübingen, Germany

[3] Departament de Geologia, Universitat Autònoma de Barcelona, 08193 Bellaterra (Cerdanyola del Vallès), Spain

[4] Departament de Mineralogia, Petrologia i Geologia Aplicada, Universitat de Barcelona, 080280 Barcelona, Spain

[5] School of Geosciences, King's College, University of Aberdeen, Aberdeen AB24 3UE, United Kingdom

[6] School of Geographical and Earth Sciences, Gregory Building, University of Glasgow, Glasgow G12 8QQ, UK

[7] Dept. Earth, Ocean and Ecological Sciences, School of Environmental Sciences, Jane Herdman Building, Liverpool University, Liverpool L69 3GP, U.K.

[8] Australian Research Council Centre of Excellence for Core to Crust Fluid Systems/GEMOC, Department of Earth and Planetary Sciences, Macquarie University, NSW 2109, Australia

[9] Henry Moseley X-ray Imaging Facility, School of Materials, The University of Manchester, M13 9PL, Manchester, UK.

[10] School of Earth, Atmosphere and Environmental Sciences, Monash University, Clayton, Vic 3800, Australia

[11] Los Alamos National Laboratory, MST8, MS G755, Los Alamos, NM, 87545, USA

[12] Centre for Exploration Targeting, School of Earth Sciences, The University of Western Australia, 35 Stirling Hwy, Crawley, 6009, Australia

Corresponding author: Sandra Piazolo (s.piazolo@leeds.ac.uk)

Abstract

This review provides an overview of the emergence and current status of numerical modelling of microstructures, a powerful tool for predicting the dynamic behaviour of rocks and ice at the microscale with consequence for the evolution of these materials at a larger scale. We emphasize the general philosophy behind such numerical models and their application to important geological phenomena such as dynamic recrystallization and strain localization. We focus in particular on the dynamics that emerge when multiple processes, which may either be enhancing or competing with each other, are simultaneously active. Here, the ability to track the evolving microstructure is a particular advantage of numerical modelling. We highlight advances through time and provide glimpses into future opportunities and challenges.

Keywords: review, evolution of microstructures, numerical modelling, dynamic recrystallization, process interaction

1. Introduction

Structural geology studies how rocks deform under applied stress or strain. These studies are applied from the sub-grain scale to that of mountain belts and tectonic plates. To know what has happened to a volume of rock millions of years ago, or to predict what would happen to a rock volume under certain (future) conditions, we need to know the link between (i) the boundary conditions (e.g. applied stress or strain, pressure-temperature conditions), (ii) the intrinsic material properties (e.g. Young's modulus, crystal symmetry, slip systems) and (iii) the processes that may be activated (e.g. dislocation creep, pressure solution, mineral phase changes). These three together determine the evolution of the state of the rock (e.g. developing cleavage, folds, lineation, stylolites) and its bulk material properties (e.g. viscosity). The microstructure is thus a *state variable* of a rock, describing the state it achieved as a result of the interplay between various processes and boundary conditions. Importantly, the microstructure is not a passive log of events, but plays an active and central role in the evolution of a rock throughout its history (Gottstein, 2004). In this context non-linear feedback between a specific microstructural configuration and local changes in intrinsic and extrinsic parameters may be important but difficult to predict. Hence, the microstructure is the link that couples the material properties, boundary conditions and processes that together control the behaviour and evolution of a rock. Consequently, the analysis and correct interpretation of microstructures is crucial in gaining an understanding of how rocks, including ice, deform on Earth and other planets. Here we define microstructure as the full spatial, compositional and orientational arrangement of all entities in a rock, typically on the scale of a thin section to hand specimen (roughly µm to cm) (Hobbs et al., 1976). These entities include minerals, grain and subgrain boundaries, crystal lattice orientations, and chemical composition from the nano- to micro-scale.

While the rock's temperature or elastic strain are ephemeral, the microstructure may be preserved for the geologist to interpret millions to billions of years later. Therefore,

74 microstructures are one of the prime forensic tools to unravel the history of a rock that allows
75 us to deduce the succession of strain rates, stresses, diagenetic and metamorphic conditions
76 and the rock's rheology during deformation (e.g. Hobbs et al., 1976; Vernon, 2004; Passchier
77 and Trouw, 2005).
78
79 One major problem in microstructural studies is that we normally only have a static record as
80 *post-mortem* "images" (grain arrangement in thin section, chemical and orientation
81 characteristics derived using electron microscopy, 3D datasets from computer tomography,
82 neutron diffraction and synchrotron beam analysis, etc.). To interpret microstructures, we
83 need to know how they form and change. Means (1977) wrote: "a more valuable kind of
84 kinematic investigation is that in which the time sequence of incremental strains or
85 incremental displacements, the kinematic *history*, is correlated with *progressive* structural
86 change. This promises to reveal more about the physics of rock deformation and to provide
87 more sensitive structural methods for reconstructing tectonic history". Such investigations
88 first became possible using *in-situ* analogue experiments that were introduced to geology by
89 influential scientists such as Cloos (1955) and Ramberg (1981), and at the microstructural
90 scale by Means (1977). In *in-situ* analogue experiments by Means (1977), inspired by those
91 of McCrone and Chen (1949), a thin-section sized sample of crystalline analogue material is
92 sandwiched and deformed between glass plates to observe the changing microstructure under
93 a microscope. These experiments were followed by a large number of studies that
94 investigated deformation related features such as dynamic recrystallization and crystal
95 plasticity (e.g. Means, 1977; 1980; Means and Ree, 1988; Park and Means, 1996; Urai et al.,
96 1980; Urai and Humphreys, 1981; Wilson, 1986; Jessell, 1986; Ree, 1991; Bons and Jessell,
97 1999; Ree and Park, 1997; Herwegh and Handy, 1996, 1998; Nama et al., 1999; Wilson et
98 al., 2014), melt or fluid-bearing microstructures (e.g. Urai, 1983; Rosenberg and Handy,

2000, 2001; Rosenberg, 2001; Schenk and Urai, 2004, 2005; Walte et al., 2005), the development of vein and fringe microstructures (e.g. Hilgers et al., 1997; Koehn et al., 2003) and the formation of δ-clasts (ten Brink et al., 1995). Many of these experiments made clear that when a polycrystalline material deforms, *multiple* processes act upon the microstructure and govern its dynamic behaviour throughout its deformation and post-deformation history (Fig. 1a; see also movies at http://www.tectonique.net/MeansCD/). In addition, pre-existing heterogeneities and/or those developing during deformation can have a significant effect on the dynamics of the system since local variations in stress and strain play a significant role in the evolution of microstructures and material behaviour, with their effects on chemistry being particularly intriguing (Wheeler, 2018).

Although changes in microstructural characteristics (e.g. grain size) can be quantified in such experiments, the underlying principles of the active processes still need to be deduced. Therefore, an additional tool is needed. Here numerical models simulating microstructural development based on several concurrent processes become important. Such numerical simulations share the advantage of *in-situ* experiments that the full microstructural development can be traced in form of time-series, with the opportunity to systematically study the effect of different processes and/or pre-existing heterogeneities on the microstructural development. In addition, numerical simulations are neither constrained by time nor specific boundary conditions. Once calibrated against laboratory experiments (e.g. Piazolo et al., 2004) or analytical solutions, they can be applied to a wide range of conditions or materials including those not attainable or suitable for laboratory experiments. In many cases, the developed microphysical behaviour may be applied to problems on the continental scale.

In this contribution, we aim to give an overview of the concepts behind numerical modelling of microstructures, i.e. microdynamic modelling, and the achievements that have been made

124 in this field. This is followed by a selection of examples of the current state of the art. Finally,
125 future possibilities and directions are briefly discussed, including some work in progress. We
126 focus on those studies that (i) are applied to geological materials, (ii) involve several
127 processes and (iii) allow prediction and visualization of the development of the
128 microstructure. Hence, we exclude studies where microstructures are not spatially mapped
129 along with models in which grains are modelled as if embedded in a medium with averaged
130 properties. Table 1 summarizes the microdynamic numerical models cited, the numerical
131 method used and processes included in each model.
132
133 ## 2. Numerical simulation of microstructures
134 ### *2. 1.* ***Emergence and philosophy***
135 Soon after the first *in-situ* experiments, computers had advanced to a stage allowing the first
136 numerical simulations of microstructural development, with a full "image" of the
137 microstructure, to appear in geology (Etchecopar, 1977; Jessell, 1988a,b; Jessell and Lister,
138 1990). When using such models we accept the fact that the scientific description of the
139 phenomena studied does not fully capture reality. This is not a shortcoming but a strength, as
140 general system behaviour and interrelationships can be studied systematically and
141 transferred to geological questions. In a numerical model the behaviour of a system emerges
142 from the piece-meal enumeration of the behaviour of each of its component parts. As a
143 consequence, numerical models are powerful and necessary when the bulk behaviour is
144 influenced by the local interaction of the components. In contrast, global, averaged or mean
145 field solutions cannot fully encompass the effect of processes that interact with each other
146 on the small scale. In nature, patterns emerge (e.g. orientation and arrangement of high-
147 strain zones, foliation, fractures) which may be used to deduce conditions of their formation.

148 Numerical models are powerful tools to investigate this link between patterns observed in
149 nature and processes that are responsible for their development.
150
151 ***2.2. Multiprocess modelling – approaches***
152 As shown convincingly by the aforementioned experiments, several processes act
153 concurrently on a microstructure and control the dynamics of the microstructural evolution
154 and material properties (e.g. Means, 1977, 1980). While there are a large number of models
155 that focus on one process alone, there are fewer systems that aim to model the effect of
156 multiple interacting processes. Here, we focus on the latter. Solving all necessary equations
157 simultaneously is only practical when the number of interacting processes is small.
158 Alternatively, the set of equations, hence processes, needs to be reduced to a manageable
159 number necessitating a user driven selection which may result in the omission of important
160 feedbacks. Operator splitting provides an alternative approach, whereby each process acts
161 sequentially on a microstructure that was incrementally changed by all operating processes in
162 the previous step. In this case, the number of equations to be solved is not limited; hence
163 there is no need to artificially reduce the number of modelled processes. Clearly, length scale
164 and time steps have to be considered carefully for this approach to be valid. The operator
165 splitting approach is fundamental to the numerical platform Elle (Jessell et al., 2001, Bons et
166 al., 2008, Piazolo et al., 2010; www.elle.ws) which is, within the realm of microdynamic
167 modelling, the most used numerical platform in geology. However, operator splitting has also
168 been employed in other numerical schemes (e.g. Cross et al., 2015).
169
170 ***2.3. The numerical representation of a microstructure***
171 It is necessary to describe numerically the microstructure so that in the model the processes
172 can act upon it spatially. Up to now, for rocks and ice, microstructural models have been

mostly restricted to two-dimensions. Two basic approaches can be taken: (i) a lattice data structure or (ii) an element data structure. In the lattice data structure, the microstructure is mapped onto an irregular or regular lattice, like the pixels in a digital image or gridded analysis points obtained during chemical mapping and orientation mapping of geological samples. Potts, cellular automata, lattice-spring, particle-in-cell, phase field and micromechanical Fast Fourier Transform (FFT) based models utilize the lattice data structure (Fig. 2; see also chapter 2 of Bons et al., 2008 for a detailed review of different numerical methods). Numerically the lattice data structure is easy to use and calculations are straightforward. In the element data structure, the microstructure is described by discrete elements which can be points, line segments, or polygons (Fig. 2). Finite-element models and boundary models typically use elements to describe a system. Element data structure is well suited for processes acting upon a surface, e.g. grain boundary migration, but is numerically more "expensive" due to necessary topology checks. Both elements and lattice points can have, in addition to their location in *xy* space, specific properties or store specific state variables, such as mineral phase, chemical composition, crystallographic orientation, and stress and strain (rate) values, respectively. The numerical platform Elle (Jessell et al., 2001) combines these two approaches: a microstructure is represented by boundary nodes connected by straight segments (Fig.2). A polygon enclosed by boundary nodes represents a grain or subgrain. Property variations within the individual polygons are defined at interior points where information is recorded and tracked. Processes acting on the microstructure can move boundaries and/or interior points and/or change the properties at those points, e.g. composition, crystallographic orientation or dislocation density. The system has now matured to a stage that it can robustly be used for a large variety of models relevant to geology.

3. Examples of modelling several coupled processes

3.1. Dynamic recrystallization

3.1.1. A historical perspective

Dynamic recrystallization is the response of a crystalline aggregate to lower its free energy by formation and movement of sub- and grain boundaries (Means, 1983). It occurs by a number of concurrent processes that act upon the polycrystalline material. For decades, geologists have used microstructural characteristics developed during dynamic recrystallization to infer dominance of processes and linked boundary conditions (e.g. Urai et al., 1986; Hirth and Tullis, 1992; Stipp et al., 2002). Following the first attempts of such a model (Etchecopar, 1977), Jessell (1988a,b) and Jessell and Lister (1990) developed a numerical model incorporating rotation of the crystal lattice and dynamic recrystallization for quartz. The data structure used was a 100x100 hexagonal lattice structure where each lattice point represented a grain or subgrain (Fig. 3a inset). Calculation of the crystal lattice rotation in Jessell and Lister (1990) uses the Taylor-Bishop-Hill calculation method (Taylor, 1938; Bishop and Hill, 1951a, 1951b; Lister and Paterson, 1979) and the critical resolved shear stress of the different slip systems in quartz. This work reproduced the general microstructures seen in a mylonite. A major step forward was that the simulations showed that dynamic recrystallization can significantly modify crystallographic preferred orientation (CPO) development. Piazolo et al. (2002) advanced Jessell's model by utilizing the more robust Elle data structure to describe the local deformation and the dynamics of the grain boundary network (Jessell et al., 2001). The model now included a finite element solution for incompressible, linear or nonlinear viscous flow (BASIL; Barr and Houseman 1992, 1996) to compute the local velocity field, the front tracking method for the motion of grain boundaries by moving nodes and segments (e.g. Bons and Urai, 1992), the Taylor-Bishop-Hill formulation (Lister and Paterson, 1979) and additional features such as crystal lattice rotation, formation of subgrains, recrystallization by nucleation, grain boundary migration, recovery, work hardening and

223 tracking of dislocation densities. This list of additional features shows the advance made in
224 approximately a decade in reproducing natural microstructures (Fig. 3b).
225 So far, the rheological anisotropy of minerals deforming by dislocation creep was not taken
226 into account in the calculation of the stress-strain rate field and lattice rotation. About another
227 decade after Piazolo et al. (2002), the viscoplastic implementation of the full-field crystal
228 plasticity micromechanical code based on Fast Fourier Transforms (VPFFT; Lebensohn,
229 2001) was introduced in geological microstructural modelling (Griera et al., 2011, 2013,
230 2015). The VPFFT is a spectral method that specifically assumes that deformation is
231 achieved by dislocation glide on crystallographic slip planes (each with their own critical
232 resolved shear stress) whose orientations are mapped on a regular grid (for details see Griera
233 et al. (2013), Montagnat et al. (2011, 2014) and Llorens et al. (2016a)). The simulations of
234 Griera et al. (2011, 2013) and Ran et al. (2018) illustrate that heterogeneous stress within and
235 between grains that emerge from inhomogeneous slip has a significant effect on the rotation
236 rate of porphyroclasts and -blasts and the strain (rate) field around these objects.
237 More recently, Llorens et al. (2016a; 2016b; 2017) and Steinbach et al. (2016; 2017) coupled
238 dynamic recrystallization (*DRX*) by grain boundary migration (*GBM*), intracrystalline
239 recovery and polygonisation with VPFFT crystal plasticity models, and applied them to study
240 the deformation of polar ice. Llorens et al. (2016a) presents a comprehensive description of
241 the method. They found that *DRX* produces large and equidimensional grains, but only
242 marginally affects the development of the c-axes CPO. However, *DRX* can alter the activity
243 of slip systems and does modify the distribution of a-axes. In simple shear, the strong
244 intrinsic anisotropic of ice crystals is transferred from the crystal to the polycrystal scale,
245 leading to strain localisation bands that can be masked by *GBM* (Llorens et al., 2016b).
246 Llorens et al. (2017) compared the dynamics of pure polar ice polycrystalline aggregates in
247 pure and simple shear deformation. It was found that, due to the vorticity of deformation, it is

248 expected that ice is effectively weaker in the lower parts of ice sheets (where simple shear
249 dominates) than in the upper parts (where ice is mostly deformed coaxially). The method was
250 also applied to reproduce the development of tilted-lattice (kink) bands found in ice cores
251 (Jansen et al., 2016) and crenulation cleavage during folding (Ran et al., 2018) as a result of
252 mechanical anisotropy. Steinbach et al. (2016) included air inclusions as a second phase to
253 simulate *DRX* in porous firn and found that *DRX* can occur despite the low strain and stress in
254 firn.
255 Apart from polar ice, the VPFFT-Elle model has also been used to analyse subgrain rotation
256 recrystallization of halite polycrystals in simple shear (Gomez-Rivas et al., 2017) by coupling
257 VPFFT with the Elle routines that simulate intracrystalline recovery (Borthwick et al, 2013)
258 and subgrain rotation. They found that recovery does not affect CPOs, but strongly decreases
259 grain size reduction. These authors also evaluated the use of mean subgrain misorientations
260 as a strain gauge.
261 3.1.2. Testing the effect of different combinations of recrystallization processes
262 We show results from three combinations of processes that occur during dynamic
263 recrystallization. These processes act on the same initial 10x10 cm aggregate of ice Ih
264 crystals (Fig. 4a). The numerical approach in these simulations is based on the VPFFT
265 micromechanical model in combination with several Elle processes (Llorens et al., 2016a,
266 2016b, 2017; Steinbach et al., 2016; 2017). The deformation-induced lattice rotation and the
267 estimation of geometrically necessary dislocation densities calculated from the stress and
268 velocity field provided by the VPFFT algorithm are used to simulate recrystallization by
269 intra-crystalline recovery, grain boundary migration and nucleation. Grain boundary
270 migration (*GBM*) is simulated based on the algorithm by Becker et al. (2008). Here, a front-
271 tracking approach is used in which the movement of boundaries is mapped through time.
272 Recovery reduces the intra-granular stored energy in a deformed crystal (Borthwick et al.,

2013). Nucleation creates new grain boundaries with areas of misorientation values above a pre-defined threshold (Piazolo et al., 2002; Llorens et al., 2017; Steinbach et al., 2017). Dextral simple shear deformation is applied in strain increments of $\Delta\gamma = 0.04$. Three different combinations of recrystallization processes are tested: (1) *GBM* only, (2) *GBM* and recovery or (3) *GBM*, recovery and nucleation (Fig. 4a). Simulations including VPFFT viscoplastic deformation show a similar evolution of c-axis orientation, regardless of the dynamic recrystallization processes included (Fig. 4a). The lack of influence of nucleation on the CPO is due to the fact that new grains are modelled to have lattice orientations close to those of their parent grains. However, inclusion of the nucleation process result in grain size reduction (Fig. 4b). Results illustrate how different combinations of microdynamic processes affect the microstructural characteristics (e.g. CPO, grain size, shape and orientation) in different ways where no single microstructural parameter can grasp the full dynamics of polycrystalline deformation.

3.2. Diffusion creep

Diffusion creep is a physico-chemical process that operates in large regions of the Earth – in the upper Earth as "pressure solution" where diffusion is enhanced along fluid films and elsewhere at low strain rates, maybe in large parts of the lower mantle (Karato, 1992). The mechanism involves diffusion driven by gradients in normal stress along boundaries. In simple models no other driving forces need to be included. It is implicit in our understanding of this mechanism that grain boundary sliding occurs in conjunction with diffusion. Ford et al. (2002) devised a numerical model to understand the evolution of grain shapes and CPO in grain boundary diffusion creep. The mathematical framework allows for the consideration of diffusion and sliding together. Operator splitting is not required and the evolution at each timestep is based on a single matrix inversion operation. The model couples the microstructure to an evolving system of local stresses (Fig. 5). The model predicts that grain

298 shapes become somewhat elongate, in accordance with experiments on calcite (Schmid et al.,
299 1987) and observations on an albite-bearing mylonite (Jiang et al., 2000) (Fig. 5). It also
300 predicts that grain rotations are not chaotic and that CPO may be present to high strains
301 (Wheeler, 2009), as seen in, for example, experiments on olivine-orthopyroxene (Sundberg
302 and Cooper, 2008) and predicted by numerical simulations of Bons and den Brok (1999). A
303 second phase, if insoluble, can be included and such a model was used by Berton et al. (2006,
304 2011) to prove the hypothesis that a different grain boundary diffusion coefficient along the
305 two-phase boundaries could explain fibre growth in pressure shadows. Not all model
306 predictions are in agreement with other investigations – for example some materials
307 deformed by diffusion creep e.g. olivine show quite equant grains (Karato et al., 1986). In
308 such experiments grain growth occurs but this process was not included in the numerical
309 model, hence results differ. In a later section we address this issue, but this example
310 illustrates that, in common with other numerical models, the applicability reflects the
311 processes included.

312 **3.3. Stress driven dissolution, growth and dynamic roughening**

313 Another example where stress leads to micro- and macrostructures is the roughening of grain
314 boundaries in the presence of a fluid. In this case dissolution and/or mineral growth are
315 driven not just by normal stress gradients at the interface (c.f. section 3.2) but also by changes
316 in elastic and surface energies. In addition to these driving forces, the detailed
317 electrochemistry of interfaces has a kinetic effect on rates (Gratier et al., 2013). In the
318 example presented here, the process is modelled in Elle by coupling a lattice spring code that
319 calculates the strain with a background fluid that dissolves lattice elements. This process can
320 produce transient patterns of interface geometry at the grain boundaries (Koehn et. al., 2006).
321 In addition, the process itself produces rough interfaces that can be seen on the larger scale as
322 stylolites (Koehn et al., 2007; Ebner et al., 2009). The scaling behaviour of stylolites is

323 important for stress inversion and compaction on the basin scale (Koehn et al., 2012; 2016)
324 and the shape of stylolites is partly rooted in the microstructure of the host-rock (Fig. 6).
325 Slower dissolving material on various scales, from small grains to fossils and layers, can
326 influence the dissolution process and thus the development of patterns, whereas deformation
327 leads to changes in long-range interactions (Koehn et al., 2016). Similarly, pinning behaviour
328 in the presence of a fluid is seen in grain growth where grain boundary pinning results in
329 restriction of grain growth. Pinning particles can also be moved around so that growing
330 grains become clean. Such a process can lead to layered rocks, for example, zebra dolomites
331 (Kelka et al., 2015).

332 **4. Numerical simulations of microdynamic processes: Examples of ongoing work**

333 **4.1.** ***Linking chemistry and microstructural evolution***

334 Even now, most of the numerical models that incorporated more than one process are
335 restricted to deformation processes alone. Although in diffusion creep there is an intrinsic
336 chemical aspect, the model described in 3.2 involves just a single phase of fixed composition.
337 There are some models that incorporate the growth of new mineral phases and investigate the
338 rheological effect of such growth (e.g. Groome et al., 2006; Smith et al., 2015), however the
339 location of new phase growth and/or growth rate is predefined. While Park et al. (2004)
340 showed convincingly the effect of microstructure on the diffusion pathways and chemical
341 patterns in garnet and biotite, there are now many opportunities available in a numerical
342 system such as Elle (Jessell et al., 2001) to couple local chemistry and microstructural
343 evolution. Below we present preliminary results from two current projects linking chemical
344 changes and a dynamically evolving grain network.

345 4.1.1. Grain boundary diffusion creep and grain growth

346 Here we present the first results using a model combining, using operator splitting,
347 deformation by diffusion creep (Ford et al., 2002; Wheeler, 2009) and surface energy driven

348 grain boundary migration (GBM), i.e. grain growth (modified after Becker et al., 2008). Four
349 different scenarios are shown: diffusion creep only, grain boundary migration only and two
350 combinations with medium and high grain boundary migration GBM rates (Fig. 7a). The
351 starting material is an almost regular hexagonal grain mesh with equant grains in which triple
352 junctions have had small random perturbations imposed (Fig. 7a). The perturbations are
353 required to avoid mathematical problems that arise in perfectly regular hexagonal networks
354 (Wheeler, 2010). Topology checks such as neighbour switching routines are performed after
355 each step in all simulations, ensuring that no topology problems arise. The microstructural
356 development is markedly different if grain growth is coupled with diffusion creep (Fig. 7a)
357 where with increasing GBM rate the aspect ratios are generally reduced relative to that of
358 comparable experiments modelling diffusion creep only. This is provisionally in accord with
359 the hypothesis that there will be a 'steady state' grain elongation developed which is a
360 function of the relative magnitudes of strain rate and grain growth kinetic parameters
361 (Wheeler, 2009) but more simulations are required (with less regular starting
362 microstructures). In contrast, for grain growth only, the microstructure does not change as the
363 initial configuration consists of stable near 120° triple junctions (Fig. 7a). Grain numbers (i.e.
364 grain size) do not change in any of the simulations.
365 4.1.2. Trace element partitioning between fluid and solid coupled with recrystallization
366 Field and experimental studies illustrate the importance of the time and length scales on the
367 evolution of grain networks during trace element diffusion (e.g. Ashley et al., 2014 and
368 references therein). Therefore, understanding the influence of recrystallization on trace
369 element distribution is essential for correctly interpreting patterns of trace element
370 distribution (e.g. Wark and Watson, 2006). However, to our knowledge there are currently no
371 numerical approaches able to simulate diffusion coupled with microstructure evolution.
372 Recently, a new Elle finite difference process that solves Fick's second law to simulate trace

element diffusion in a polycrystalline medium has been developed. The polycrystal is defined by *n*-phases where grain boundaries and grains are differentiated (Fig. 7b). The trace element partitioning coefficient between different phases is also considered. The approach uses an element data structure representing grain boundaries and a lattice data structure of a regular grid of unconnected lattice point to track diffusion along the grain boundaries and the physical and chemical properties within grains, respectively. To ensure elemental exchange between grain boundaries and grain interiors, a grain interior-grain boundary partition coefficient is implemented that takes the proximity to grain boundaries into account. This allows the simulation of coupled bulk and grain boundary diffusion. This approach can be fully coupled with other processes of the numerical platform Elle and therefore allows simulating simultaneous diffusion, deformation and static or dynamic recrystallization. The use of this approach is demonstrated through the modelling of diffusion of a tracer with fractionation during static grain growth of a single-phase aggregate (Fig. 7b) (after that presented by Jessell et al., 2001). Patterns of chemical concentration qualitatively resemble those of Ti-distribution observed in recrystallized quartz in shear zones and can help to understand the redistribution of Ti in quartz during dynamic recrystallization (e.g. Grujic et al., 2011), among many other geological problems.

4.2. *Modelling in three dimensions*

We restricted this review to two-dimensional numerical approaches, as very few models have been published that are in three dimensions and also specific to geological microstructures. An exception is the phase field approach by Ankit et al. (2015) who investigate the growth of crystals in an open fracture. However, within the material science community numerical models exist that investigate the behaviour of a microstructure in response to single processes in three dimensions (e.g. three dimensional crystal plasticity modelling platform DAMASK (Roters et al., 2012; Eisenlohr et al., 2013), which includes the option of solving the

micromechanical problem using a 3D implementation of the FFT-based formulation (presently implemented in Elle in its 2-D version) and grain growth (e.g. Krill and Chen, 2002; Kim et al., 2006). With the technical advances made within the geological and material science community it is now in principle possible to extend currently available 3D models to geological questions and/or multi-process scenarios.

4.2.1. Dissolution of reactive surfaces in three dimensions

Mineral dissolution controls important processes in geoscience such as serpentinization (e.g. Seyfried et al., 2007), retrogression and replacement reactions (Putnis and Austrheim, 2012), deformation by dissolution-precipitation creep (e.g. Rutter, 1976) and also affects processes relevant to society such as the stability of spent nuclear fuel and mine waste. Recent work has shown that dissolution rates are linked to the evolving surface structure, and thus are time-dependent (Godinho et al., 2012). Different surfaces have different structures in three dimensions and the presence of etch pits play a major role in dissolution (Pluemper et al., 2012). Hence, for accurate representation of dissolution behaviour, modelling in three dimensions is important. Here, we present a numerical model that simulates the dissolution process as a potential tool to quantify the links between dissolution rates, reactive surface area and topography over periods of time beyond reasonable for a laboratory experiment. The program uses empirical equations that relate the dissolution rate of a point of the surface with its crystallographic orientation (Godinho et al., 2012) to simulate changes of topography during dissolution, which ultimately results in the variation of the overall dissolution rate (Godinho et al., 2012, 2014). The initial surface is composed of a group of nodes with a xy position and a set height (z). For each lattice point a local surface orientation is calculated from the inclination of the segment node and its neighbours. This orientation together with the crystallographic orientation of the grain the surface belongs to is then used to calculate a dissolution rate (surface reactivity). Based on this the displacement of the node using the

423 equations published in Godinho et al. (2012) is calculated. The model allows the graphical
424 display of the three-dimensional topographic development of the surface, tracking of the
425 variation of the surface area and calculation of the overall dissolution rate at each stage of the
426 simulation. Results obtained with the 3D simulation at three consecutive stages of dissolution
427 (150 hrs, 180 hrs, 276 hrs dissolution duration) show that numerical results are in accordance
428 to experimental results (Fig. 7c).
429

430 **5. Numerical simulations of microstructures: Possibilities and challenges**

431 ***5.1. Linking laboratory and natural data with numerical models***

432 Over the last two decades numerical capabilities have advanced markedly and models have
433 come of age. Consequently, a large range of models and process combinations is now
434 available that can be utilized to gain further insight into the link between processes, material
435 properties and boundary conditions. This also includes polymineralic systems making the
436 models more appropriate to use to investigate processes occurring within polyphase rocks
437 (e.g. Roessiger et al., 2014; Steinbach et al, 2016). New avenues of effective verification
438 against laboratory and natural data are now opening up, due to the development of analytical
439 tools allowing rapid complete microstructural and microchemical analysis providing dataset
440 similar to those possible in numerical models (e.g. Steinbach et al, 2017, Piazolo et al., 2016);
441 many of the analytical data sets have a lattice data structure.

442 ***5.2. Linking chemistry and microstructural evolution***

443 Advances in numerical methods, theoretical treatment of thermodynamic data, analytical
444 tools and theoretical and experimental insights into the coupling between chemical and
445 physical process that emerged over the last decade, call for a major effort in this area of
446 research. Examples of areas of opportunities include investigation of the (1) significance of
447 local stress versus bulk stress on mineral reactions and reaction rates (e.g. Wheeler, 2014), (2)

448 characteristics of replacement microstructures and their potential significance for
449 microstructural interpretation (e.g. Putnis, 2009, Spruzeniece et al., 2017), (3) mobility of
450 trace elements enhanced by deformation that change significantly the local elemental
451 distributions (e.g. Reddy et al., 2007, Piazolo et al., 2012, 2016) and (4) coupling between
452 reactive fluid-solid systems and hydrodynamics (Kelka et al., 2017). Increasing computer
453 processing speeds will aid the running of such models. However, the technical challenges
454 include the harmonisation of fundamentally different numerical approaches (crystal plasticity
455 versus diffusion creep, for example) and the resolution of fundamental mathematical
456 problems, e.g. the current lack of an internally consistent model for multiphase diffusion
457 creep, highlighted by Ford and Wheeler (2004).

458 ***5.3. Linking brittle and ductile deformation: elasto-viscoplastic behaviour***

459 When examining the rock record, it is clear that in many cases, brittle and ductile behaviour
460 often occurs at the same time within a rock (e.g. Bell and Etheridge, 1973, Hobbs et al.,
461 1976). With the potential significance of grain-scale brittle behaviour now measurable on
462 seismic signals (e.g. Fagereng et al., 2014) there is an increased need in developing numerical
463 techniques that allow us to model the dynamic link between brittle and ductile behaviour.
464 Such elasto-viscoplastic behaviour combines the elastic reversible fast deformation with a
465 viscous time dependent flow and a plastic behaviour. These behaviours can be included in
466 continuous or discontinuous models. For example, in the numerical platform Elle, a lattice
467 structure is used to deform the model elastically up to a critical stress where bonds fracture
468 (plastic behaviour) and the particles themselves deform as a function of stress and time
469 (viscous behaviour). In this case the viscous behaviour conserves the volume whereas shear
470 forces and differential stresses converge to zero (Sachau and Koehn, 2010, 2012; Arslan et
471 al., 2012; Koehn and Sachau, 2014). Alternatively, linking the elasto-visocplastic FFT based
472 (EVPFFT) (Lebensohn et al., 2012) with models such as Elle would allow calculation of the

473 Cauchy stresses that are the local driving force for grain scale damage processes.
474 One of the major challenges is the large range of time-scales in these processes, with
475 fracturing and fluid flow on fast to intermediate and viscous deformation and potentially
476 reactions on very long time scales. This complexity either requires the assumption that some
477 processes are instantaneous or it requires an "up-scaling in time" or non-linear time scales in
478 models.
479
480 ***5.4. Expansion of capability to three dimensions***
481 With the advent of supercomputers and new numerical approaches now is the time to develop
482 techniques to investigate microstructural development in three dimensions. This is of
483 particular importance if material transport such as aqueous fluid and/or melt flow is to be
484 considered. This would enable, for example, modelling of strain fringes, shear veins and en-
485 echelon tension gashes. However, these require models that link brittle and ductile behaviour
486 along with modelling in three dimensions.
487 One of the biggest problems faced with three-dimensional models of microstructures are the
488 three-dimensional topology changes that are common in dynamic microstructural
489 development (e.g. Fig. 1-7). This is a major problem if an element data structure with
490 segments, i.e. grain boundaries is used. However, the phase field approach does not work
491 with such distinct boundaries, and is therefore well suited for 3D problems (e.g. Ankit et al.
492 2014). In addition, a three dimensional network of unconnected nodes, in which there is no
493 physical movement of boundaries but only changes in the properties of the 3D nodes (voxels)
494 (cf. Fig. 7c) may be a way forward (e.g. Sachau and Koehn, 2012).
495
496 ***5.5. Link between geophysical signals and microstructure***

497 At a time where there is an ever-increasing amount of geophysical data being collected,
498 numerical simulations that are used to test the link between microstructural development and
499 geophysical signal will become increasingly important. Cyprych et al. (2017) showed that not
500 only crystallographic preferred orientation but also the spatial distribution of phases i.e. the
501 microstructure, has a major impact on seismic anisotropy. Therefore, a direct link between
502 the microdynamic models such as Elle allowing tracking of microstructural changes through
503 time and space and geophysical signal generation offers a wealth of new opportunities
504 including interpretation of strong reflectors in the lower crust and mantle. Current efforts by
505 Johnson, Gerbi and co-workers (Naus-Thijsen et al., 2011; Cook et al., 2013; Vel et al., 2016)
506 are in line with this direction.
507
508 ***5.6. Application of numerical models to polymineralic rock deformation and ice-related***
509 ***questions***
510 The dynamic behaviour of the Earth is strongly influenced by the deformation of
511 polymineralic rocks. At the same time Earth's polar ice caps and glacial ice which often
512 include ice and a second phase (e.g. air inclusions, dust, entrained bedrock) is of major
513 importance to society, especially in view of changing climate (e.g. Petit et al., 1999; EPICA,
514 2004). Application of the current numerical capabilities to polycrystalline ice and
515 polymineralic rocks is therefore urgently needed. Over the last years, there has been an
516 increased effort in this direction (Roessiger et al., 2011, 2014; Piazolo et al., 2015; Llorens et
517 al., 2016a, 2016b, 2017; Jansen et al., 2016; Steinbach et al. 2016, 2017), which promises to
518 continue. Here, the development of the link between elemental mobility and microstructural
519 development is of major importance, as only with such models the can chemical signals of,
520 for example, ice cores be correctly interpreted.
521

5.7. Upscaling: Utilizing operator splitting and utilities developed for microdynamic systems to larger-scale problems

One of the strengths of the numerical approach taken by the microstructural community has been the close link between different processes and the ability of the models to take into account the local differences in properties such as stress, strain and chemistry. The technique of operator splitting has proven extremely powerful. Furthermore, the ability to model anisotropic material behaviour utilizing for example VPFFT viscoplastic deformation formulations (Lebensohn, 2001), has enabled realistic and dynamic models. Upscaling this approach to investigate problems at a large scale e.g. folding (Llorens et al., 2013a, 2013b; Bons et al., 2016; Ran et al., 2018) and shear deformation (Gardner et al., 2017) have shown to be very beneficial. There is great scope to expand further on this in view of fluid flow, mineralization and fault formation.

6. Numerical simulations of microstructures: Lessons learnt and future challenges

Numerical simulations of microstructural development have caught our imagination over the last three decades. They have markedly advanced our ability to explain phenomena and patterns we observe in nature and experiments by allowing us to test the link between boundary conditions, material properties, processes, and microstructural development. Importantly, models, especially those that couple several process and/or investigate pre-existing heterogeneities can train the geologist to think of the dynamics of the system rather than a linear development. For example, different patterns of strain localization observed in nature can be explained by differences in the relative rates of interacting processes (e.g. Jessell et al., 2005; Gardner et al., 2017). At the same time, specific indicative microstructural parameters can be developed to help interpret natural microstructures (e.g. Piazolo et al., 2002; Gomez-Rivas et al., 2017, Llorens et al., 2017; Steinbach et al., 2017).

However, including chemistry coupled to other processes remains a particular challenge. Whilst, for example, trace-element diffusion can be enacted in parallel with other processes (section 4.1.2), chemical transport of major elements and diffusion creep cannot yet be fully integrated with many other processes. Indeed, when multiphase systems are considered, there are unsolved problems with diffusion creep modelling even in the absence of other processes (Ford and Wheeler, 2004). This challenge is closely linked to our current inability to confidently model grain boundary sliding.

Nevertheless, the studies we describe have shown that numerical models are extremely powerful in providing benchmark results to investigate what kind of microstructure may develop under certain conditions. These models are sophisticated mind experiments that are firmly based on physical and chemical laws for which the theory is well known individually but their interaction is difficult to predict analytically.

Acknowledgements:

We would like to thank Win Means for opening up a whole new perspective on microstructures with his inspirational in-situ experiments. The authors thank the DFG, ARC, ESF, NSF, EU through Marie Curie Fellowship to SP, the Government of Catalonia's Secretariat for Universities and Research for a Beatriu de Pinós fellowship to EGR (2016 BP 00208), and NERC (NERC grant NE/M000060/1) for support of the numerical endeavours. The authors thank C. Gerbi for his helpful and constructive review as well as C. Passchier for editorial handling of the manuscript.

References

571 Ankit, K., Urai, J. L., Nestler, B. 2015. Microstructural evolution in bitaxial crack- seal
572 veins: A phase-field study. Journal of Geophysical Research 120, 3096-3118.
573 Arslan, A., Koehn, D., Passchier, C.W., Sachau, T. 2012. The transition from single layer to
574 foliation boudinage: A dynamic modelling approach. Journal of Structural Geology 42,
575 118-126.
576 Ashley, K.T., Carlson, W.D., Law, R.D., Tracy, R.J. 2014. Ti resetting in quartz during
577 dynamic recrystallization: mechanisms and significance. American Mineralogist 99, 2025-
578 2030.
579 Barr, T.D., Houseman, G.A. 1992. Distribution of deformation around a fault in a non-linear
580 ductile medium. Geophys Res Lett 19, 1145-1148.
581 Barr, T.D., Houseman, G.A. 1996. Deformation fields around a fault embedded in a non-
582 linear ductile medium. Geophys J Int 125, 473-490.
583 Becker, J.K., Bons, P.D., Jessell, M.W. 2008. A new front-tracking method to model
584 anisotropic grain and phase boundary motion in rocks. Computers & Geosciences 34, 201-
585 212.
586 Bell, T. H., Etheridge, M. A. 1973. Microstructure of mylonites and their descriptive
587 terminology. Lithos 6, 337-348.
588 Berton, J. R., Durney, D. W., Wheeler, J., Ford, J. M., 2006. Diffusion-creep modelling of
589 fibrous pressure-shadows. Tectonophysics 425, 191-205.
590 Berton, J. R., Durney, D. W., Wheeler, J., 2011. Diffusion-creep modelling of fibrous
591 pressure-shadows II: influence of inclusion size and interface roughness. In: Deformation
592 Mechanisms, Rheology & Tectonics: Microstructures, Mechanics & Anisotropy (eds
593 Prior, D. J., Rutter, E. H. & Tatham, D.), Geological Society Special Publications, 360,
594 .319-328, .

595 Bishop J.F.W., Hill R. 1951a. A theory of the plastic distortion of a polycrystalline aggregate
596 under combined stresses. Philosophical Magazine 42, *414–427.*
597 Bishop, J.F.W., Hill, R. 1951b A Theoretical Derivation of the Plastic Properties of a
598 Polycrystalline Face-Centred Metal. Philosophical Magazine 42, 1298-1307.
599 Bons, P.D., den Brok, S.W.J. 2000. Crystallographic preferred orientation development by
600 dissolution-precipitation creep. Journal of Structural Geology 22, 1713-1722.
601 Bons, P.D., Jessell, M.W. 1999. Micro-shear zones in experimentally deformed
602 octachloropropane. Journal of Structural Geology 21, 323-334.
603 Bons, P.D., Urai J.L. 1992. Syndeformational grain growth: microstructures & kinetics.
604 Journal of Structural Geology 14, 1101-1109.
605 Bons, P.D., Koehn, D., Jessell, M.W. (Eds) (2008) Microdynamic Simulation. Lecture Notes
606 in Earth Sciences 106, Springer, Berlin. 405 pp. ISBN 978-3-540-44793-1.
607 Bons, P.D., Jansen, D., Mundel, F., Bauer, C.C., Binder, T., Eisen, O., Jessell, M.W.,
608 Llorens, M.G., Steinbach, F., Steinhage, D. Weikusat, I., 2016. Converging flow and
609 anisotropy cause large-scale folding in Greenland's ice sheet. Nature communications 7,
610 11427.
611 Borthwick, V., Piazolo, S., Evans, L., Griera, A., Bons, P.D. 2013. What happens to
612 deformed rocks after deformation? A refined model for recovery based on numerical
613 simulations. In: "Deformation Structures and Processes within the Continental Crust",
614 Special Volume 394, Geol. Soc. London. doi: 10.1144/SP394.11
615 Cloos, E. 1955. Experimental analysis of fracture patterns. Geological Society of America
616 Bulletin 66, 241-256.
617 Cook, A., Vel., S., Johnson, S.E., Gerbi, C., Song, W.J., 2013, Elastic and Seismic Properties
618 (ESP) Toolbox (beta version), http://umaine.edu/mecheng/faculty-andstaff/
619 senthil-vel/software/ESP_Toolbox/

620 Cross, A. J., Ellis, S., Prior, D. J. 2015. A phenomenological numerical approach for
621 investigating grain size evolution in ductiley deforming rocks. Journal of Structural
622 Geology 76, 22-34.
623 Cyprych, D., Piazolo, S., Almqvist, B.S.G. 2017. Seismic anisotropy from compositional
624 banding in granulites from the deep magmatic arc of Fiordland, New Zealand, Earth and
625 Planetary Science Letters 477, 156-167.
626 Ebner, M., Koehn, D., Toussaint, R, Renard, F. 2009. The influence of rock heterogeneity on
627 the scaling properties of simulated and natural stylolites. Journal of Structural Geology 31,
628 72-82.
629 Eisenlohr, P., Diehl, M., Lebensohn, R.A., Roters, F., 2013. A spectral method solution to
630 crystal elasto-viscoplasticity at finite strains. International Journal of Plasticity 46, 37-53.
631 EPICA Community members (2004) Eight glacial cycles from an Antarctic ice core. Nature
632 429, 623-628.
633 Etchecopar, A. 1977. A plane kinematic model of progressive deformation in a
634 polycrystalline aggregate. Tectonophysics 39, 121-139.
635 Fagereng, Å., Hillary, G. W. B., Diener, J. F. A. 2014. Brittle-viscous deformation, slow slip
636 and tremor. Geophysical Research Letters 41, 4159-4167.
637 Ford, J. M., Wheeler, J., 2004. Modelling interface diffusion creep in two-phase materials.
638 Acta Materialia 52, 2365-2376.
639 Ford, J. M., Wheeler, J., Movchan, A. B., 2002. Computer simulation of grain boundary
640 creep. Acta Materialia 50, 3941-3955.
641 Ford, J.M., Ford, N.J., Wheeler, J. 2004. Simulation of grain boundary diffusion creep:
642 analysis of some new numerical techniques: Proc R Soc, London 460, 2395-2413

643 Gardner, R., Piazolo, S**.,** Evans, L., Daczko, N. 2017. Patterns of strain localization in
644 heterogeneous, polycrystalline rocks - a numerical perspective, Earth and Planetary
645 Science Letters*,* 463*,* 253-265.
646 Gratier, J.P., Dysthe, D.K., Renard, F., 2013. The Role of Pressure Solution Creep in the
647 Ductility of the Earth's Upper Crust, in: Dmowska, R. (Ed.), Advances in Geophysics, Vol
648 54. Elsevier, Amsterdam, pp. 47-179.
649 Griera, A., Bons, P.D., Jessell, M.W., Lebensohn, R.A., Evans, L., Gomez-Rivas, E. 2011.
650 Strain localization and porphyroclast rotation. Geology 39, 275-278.
651 Griera, A., Llorens, M.-G., Gomez-Rivas, E., Bons, P.D., Jessell, M.W., Evans, L.A.,
652 Lebensohn, R. 2013. Numerical modelling of porphyroclast and porphyroblast rotation in
653 anisotropic rocks. Tectonpophysics 587, 4-29,
654 Griera, A., Gomez-Rivas, E., Llorens, M.-G.**,** Bons, P.D., Lebensohn, R. 2015.
655 Microstructural evolution of polycrystalline materials in simple shear: insights from full-
656 field numerical simulations**.** *Geotectonic Research* 97, 37–39.
657 Gottstein, G. 2004. Integral materials modelling. Modelling and Simulation in Materials
658 Science and Engineering, 12, I.
659 Godinho, J.R., Piazolo, S., Evans, L., 2014. Simulation of surface dynamics during
660 dissolution as a function of the surface orientation: Implications for non-constant
661 dissolution rates. Earth and Planetary Science Letters 408, 163-170.
662 Godinho, J.R.A., Piazolo, S., Evins, L.Z. 2012. Effect of surface orientation on dissolution
663 rates and topography of CaF 2, *Geochimica et Cosmochimica Acta* **86**, 392-403.
664 Gomez-Rivas, E., Griera, A., Llorens, M-.G., Bons, P.D., Lebensohn, R.A., and Piazolo, S.
665 (2017). Subgrain rotation recrystallization during shearing: insights from full-field
666 numerical simulations of halite polycrystals. Journal of Geophysical Research, in press.

667 Grujic, D., Stipp, M., Wooden, J.L., 2011. Thermometry of quartz mylonites: Importance of
668 dynamic recrystallization on Ti- in- quartz reequilibration. Geochemistry, Geophysics,
669 Geosystems, 12.
670 Groome, W. G., Johnson, S. E., Koons, P. O. 2006. The effects of porphyroblast growth on
671 the effective viscosity of metapelitic rocks: implications for the strength of the middle
672 crust. Journal of Metamorphic Geology 24: 389–407.
673 Herwegh, M., Handy, M. R. 1998. The evolution of high-temperature mylonitic microfabrics:
674 Evidence from simple shearing of a quartz analogue (norcamphor). J. Struct. Geol. 18,
675 689-710.
676 Herwegh, M., Handy M. R.. 1998 The origin of shape preferred orientations in mylonite:
677 inferences from in-situ experiments on polycrystalline norcamphor. Journal of Structural
678 Geology 20, 681-694.
679 Hilgers, C., Urai, J.L., Post, A.D., Bons, P.D. 1997. Fibrous vein microstructures:
680 Experimental and numerical simulation. Aardkundige Mededelingen 8, 107-109.
681 Hirth, G., Tullis, J. 1992. Dislocation creep regimes in quartz aggregates. Journal of
682 Structural Geology 14, 145 - 159.
683 Hobbs B.E., Means W.O., Williams P.F. 1976. An Outline of Structural Geology. John Wiley
684 and Sons, 571 pp.
685 Jansen, D., Llorens, M.-G., Westhoff, J., Steinbach, F., Kipfstuhl, S., Bons, P.D., Griera, A.,
686 Weikusat, I. 2016. Small-scale disturbances in the stratigraphy of the NEEM ice core:
687 observations and numerical model simulations. *The Cryosphere* 10, 359-370.
688 Jiang, Z., Prior, D. J., Wheeler, J., 2000. Albite crystallographic preferred orientation and
689 grain misorientation distribution in a low-grade mylonite: implications for granular flow.
690 Journal of Structural Geology 22, 1663-1674.

691 Jessell, M.W. 1986. Grain boundary migration and fabric development in experimentally
692 deformed octachloropropane. Journal of Structural Geology 8, 527-542.
693 Jessell, M. W. 1988a. Simulation of fabric development in recrystallizing aggregates—I.
694 Description of the model. Journal of Structural Geology 10, 771-778.
695 Jessell, M. W. 1988b. Simulation of fabric development in recrystallizing aggregates—II.
696 Example model runs. Journal of Structural Geology 10, 779-793.
697 Jessell, M. W., Lister, G. S. 1990. A simulation of the temperature dependence of quartz
698 fabrics. Geological Society, London, Special Publications 54, 353-362.
699 Jessell, M., Bons, P.D., Evans, L., Barr, T., Stüwe, K. 2001. Elle: the numerical simulation of
700 metamorphic and deformation microstructures. Computers And Geosciences 27, 17-30,
701 http://dx.doi.org/10.1016/S0098-3004(00)00061-3
702 Jessell, M.W., Siebert, E., Bons, P.D., Evans, L., Piazolo, S. 2005. A new type of numerical
703 experiment on the spatial and temporal patterns of localization of deformation in a
704 material with a coupling of grain size and rheology. Earth and Planetary Science Letters
705 239, 309-326.
706 Karato, S. I., Paterson, M. S., Fitz Gerald, J. D., 1986. Rheology of synthetic olivine
707 aggregates: influence of grain size and water. Journal of Geophysical Research 91, 1851-
708 8176.
709 Karato, S.I., Li, P., 1992. Diffusion creep in perovskite: implications for the rheology of the
710 lower mantle. Science 255, 1238.
711 Kelka, U., Koehn, D., Beaudoin, N. 2015. Zebra pattern in rocks as a function of grain
712 growth affected by second-phase particles. Frontiers in Physics 3, 74.
713 Kelka, U., Veveakis, M., Koehn, D., Beaudoin, N., 2017. Zebra rocks: compaction waves
714 create ore deposits. Scientific Reports 7, 14260.

715 Kim, S. G., Kim, D. I., Kim, W. T., Park, Y. B. 2006. Computer simulations of two-
716 dimensional and three-dimensional ideal grain growth. Physical Review E 74, 061605.
717 Koehn, D., Bons, P.D., Passchier, C.W. 2003. Development of antitaxial strain fringes during
718 non-coaxial deformation: an experimental study. Journal of Structural Geology 25, 263-
719 275.
720 Koehn, D., Renard, F., Toussaint, R., Passchier, C. 2007. Growth of stylolite teeth patterns
721 depending on normal stress and finite compaction. Earth and Planetary Science Letters,
722 257, 582-595.
723 Koehn, D., Ebner, M., Renard, F., Toussaint, R., Passchier, W. 2012. Modelling of stylolite
724 geometries and stress scaling. Earth and Planetary Science Letters 341, 104-113.
725 Koehn, D., Sachau, T. 2014. Two-dimensional numerical modeling of fracturing and shear
726 band development in glacier fronts. Journal of Structural Geology 61, 133-142.
727 (doi:10.1016/j.jsg.2012.11.002).
728 Koehn, D., Rood, M.P., Beaudoin, N. , Chung, P., Bons, P.D., Gomez-Rivas, E. (2016) A
729 new stylolite classification scheme to estimate compaction and local permeability
730 variations. Sedimentary Geology 346, 60-71.
731 Krill Iii, C. E., Chen, L. Q. 2002. Computer simulation of 3-D grain growth using a phase-
732 field model. Acta Materialia 50, 3059-3075.
733 Lebensohn, R. A. 2001. N-site modeling of a 3D viscoplastic polycrystal using fast Fourier
734 transform. Acta Materialia 49, 2723-2737.
735 Lebensohn, R.A., Kanjarla, A.K., Eisenlohr, P., 2012. An elasto-viscoplastic formulation
736 based on fast Fourier transforms for the prediction of micromechanical fields in
737 polycrystalline materials. International Journal of Plasticity 32, 59-69.
738 Lister GS, Paterson MS 1979. The simulation of fabric development during plastic
739 deformation and its application to quartzite: fabric transitions. J Struct Geol 1, 99-115.

740 Llorens, G.-M., Griera, A., Weikusat, I., Bons, P.D., Roessiger, J., Lebensohn, R.A. 2016a.
741 Dynamic recrystallisation of ice aggregates during co-axial viscoplastic deformation: a
742 numerical approach. Journal of Glaciology 62, 359-377.
743 Llorens, G.-M., Griera, A., Bons, P.D., Lebensohn, R.A., Evans, L.A., Jansen, D., Weikusat,
744 I. 2016b. Full-field predictions of ice dynamic recrystallisation under simple shear
745 conditions. Earth and Planetary Science Letters 450, 233-242.
746 Llorens, M. -G., Griera, A., Steinbach, F., Bons, P. D., Gomez-Rivas, E., Jansen, D.,
747 Roessiger, J., Lebensohn, R. A. and Weikusat, I. 2017. Dynamic recrystallization during
748 deformation of polycrystalline ice: insights from numerical simulations. Phil. Trans. R.
749 Soc. A 375, 20150346.
750 Llorens, M.G., Bons, P.D., Griera, A., Gomez-Rivas, E. and Evans, L.A., 2013a. Single layer
751 folding in simple shear. Journal of Structural Geology 50, 209-220.
752 Llorens, M-.G., Bons, P.D., Griera, A. Gomez-Rivas, E. 2013b. When do folds unfold during
753 progressive shear?**.** *Geology* 41, 563-566
754 McCrone WC, Chen PT .1949. Grain growth in octochloropropane. J Appl Phys 20, 230-231.
755 Means, W.D. 1977. A deformation experiment in transmitted light. Earth Planet. Sci. Letts.,
756 35, 169-179.
757 Means W.D. 1980. High temperature simple shearing fabrics: a new experimental approach.
758 J. Struct. Geol. 2, 197-202.
759 Means W.D. 1983. Microstructure and micromotion in recrystallization flow of
760 octachloropropane: a first look. Geol. Rundsch. 72, 511-528.
761 Means, W. D., Ree, J. H. 1988. Seven types of subgrain boundaries in
762 octachloropropane. Journal of Structural Geology 10, 765-770.

763 Montagnat, M., Blackford, J.R., Piazolo, S., Arnaud, L., Lebensohn, R.A., 2011.
764 Measurements and full-field predictions of deformation heterogeneities in ice. Earth and
765 Planetary Science Letters 305, 153-160.
766 Montagnat, M., Castelnau, O., Bons, P.D., Faria, S.H., Gagliardini, O., Gillet-Chaulet, F.,
767 Grennerat, F., Griera, A., Lebensohn, R.A., Moulinec, H., Roessiger, J., Suquet, P. 2014.
768 Multiscale modeling of ice deformation behavior. Journal of Structural Geology 61, 78-
769 108.
770 Nama, T.N., Otoh, S., Masuda, T. , 1999. In-situ annealing experiments of octachloropropane
771 as a rock analogue: kinetics and energetics of grain growth. Tectonophysics 304, 57-70.
772 Naus-Thijssen, F.M., Goupee, A.J., Johnson, S.E., Vel, S.S., Gerbi, C., 2011. The influence
773 of crenulation cleavage development on the bulk elastic and seismic properties of
774 phyllosilicate-rich rocks. Earth and Planetary Science Letters 311, 212-224.
775 Park Y, Means WD. 1996. Direct observation of deformation processes in crystal mushes. J
776 Struct Geol 18, 847-858.
777 Park, Y., Park, D., Evans, L., Ree, J. H. 2004. An Elle-based 2-D model for cation exchange
778 reaction between garnet and biotite. Journal of the Virtual Explorer 15.
779 Passchier, C.W., Trouw, R.A.J., 2005. Microtectonics (2nd enlarged edition). Springer
780 Verlag, Berlin.
781 Petit, J.R., J. Jouzel, D. Raynaud, N.L. Barkov, J.-M. Barnola, I. Basile, M. Bender, J.
782 Chappellaz, M. Davis, G. Delaygue, M. Delmotte, V. M. Kotlyakov, M. Legrand, V.Y.
783 Lipenkov, C. Lorius, L.Pépin, C. Ritz, E.Saltzman, M. Stievenard 1999, Climate and
784 atmospheric history of the past 420,000 years from the Vostok ice core, Antarctica. Nature
785 399, 429-436.

786 Piazolo, S., Austrheim, H., Whitehouse, M., 2012. Brittle-ductile microfabrics in naturally
787 deformed zircon: Deformation mechanisms and consequences for U-Pb dating. American
788 Mineralogist 97, 1544-1563.
789 Piazolo, S., Bons, P.D., Jessell, M.W., Evans, L., Passchier, C.W. 2002. Dominance of
790 microstructural processes and their effect on microstructural development: insights from
791 numerical modelling of dynamic recrystallization. Geol. Soc, London, Spec. Publ. 200,
792 149-170.
793 Piazolo, S., Jessell, M. J., Prior, D. J., Bons, P. D. 2004. The integration of experimental in-
794 situ EBSD observations and numerical simulations: a novel technique of microstructural
795 process analysis. Journal of Microscopy, 213, 273-284.
796 Piazolo, S., Jessell, M.W., Bons, P.D., Evans, L., Becker, J.K. 2010. Numerical simulations
797 of microstructures using the Elle platform: A modern research and teaching tool. Journal
798 of the Geological Society of India 75, 110-127.
799 Piazolo, S., La Fontaine, A., Trimby, P., Harley, S., Yang, L., Armstrong, R. and Cairney,
800 J.M., 2016. Deformation-induced trace element redistribution in zircon revealed using
801 atom probe tomography. Nature communications, 7. Piazolo, S., Kaminsky, F.V., Trimby,
802 P., Evans, L., Luzin, V., 2016. Carbonado revisited: Insights from neutron diffraction,
803 high resolution orientation mapping and numerical simulations. Lithos 265, 244-256.
804 Piazolo, S., Montagnat, M., Grennerat, F., Moulinec, H., Wheeler, J., 2015. Effect of local
805 stress heterogeneities on dislocation fields: examples from transient creep in
806 polycrystalline ice. Acta Materialia 90, 303-309.
807 Plümper, O., Røyne, A., Magrasó, A., Jamtveit, B. 2012. The interface-scale mechanism of
808 reaction-induced fracturing during serpentinization. Geology 40, 1103-1106.
809 Putnis, A. 2009. Mineral replacement reactions. Reviews in mineralogy and geochemistry 70,
810 87-124.

811 Putnis, A., Austrheim, H. 2010. Fluid- induced processes: metasomatism and
812 metamorphism. Geofluids 10, 254-269.
813 Ramberg, H., 1981. Gravity, deformation, and the earth's crust: In theory, experiments, and
814 geological application. Academic press.
815 Ran, H., de Riese, T., Llorens, M.-G., Finch, M., Evans, L.A., Gomez-Rivas, E., Griera, A.,
816 Jessell, M.W., Lebensohn, R.A., Piazolo, S., and Bons, P.D. 2018. Time for anisotropy:
817 The significance of mechanical anisotropy for the development of deformation structures.
818 Journal of Structural Geology, in press.
819 Ree, J. H., Park, Y., 1997. Static recovery and recrystallization microstructures in sheared
820 octachloropropane. Journal of Structural Geology 19, 1521–1526.
821 Reddy, S. M., Timms, N. E., Pantleon, W., Trimby, P. 2007. Quantitative characterization of
822 plastic deformation of zircon and geological implications. Contributions to Mineralogy
823 and Petrology 153, 625-645.
824 Roessiger, J., Bons, P.D., Griera, A., Jessell, M.W., Evans, L. Montagnat, M., Kipfstuhl, S.,
825 Faria, S.H., Weikusat, I. 2011. Competition between grain growth and grain size reduction
826 in polar ice. Journal of Glaciology 57 942-948.
827 Roessiger, J., Bons, P.D., Faria, S.H. 2014. Influence of bubbles on grain growth in ice.
828 Journal of Structural Geology 61, 123-132.
829 Rosenberg, C. L. 2001. Deformation of partially molten granite: a review and comparison of
830 experimental and natural case studies. International Journal of Earth Sciences 90, 60-76.
831 Rosenberg, C.L., Handy, M.R. 2000. Syntectonic melt pathways during simple shearing of a
832 partially molten rock analogue (Norcamphor- Benzamide). J. Geophys. Res. 105, 3135-
833 3149.

834 Rosenberg, C.L., Handy, M.R. 2001. Mechanisms and orientation of melt segregation paths
835 during pure shearing of a partially molten rock analog (norcamphor–benzamide). J. Struct.
836 Geol. 23, 1917-1932.
837 Roters, F., P. Eisenlohr, C. Kords, D. D. Tjahjanto, M. Diehl, D. Raabe. 2012. DAMASK:
838 the Düsseldorf Advanced MAterial Simulation Kit for studying crystal plasticity using an
839 FE based or a spectral numerical solver. Procedia IUTAM 3, 3-10.
840 Rutter, E.H., 1976. The kinetics of rock deformation by pressure solution. Philosophical
841 Transactions of the Royal Society, London, 203-219.
842 Sachau, T., Koehn, D. 2010. Faulting of the lithosphere during extension and related rift-
843 flank uplift: a numerical study. International Journal of Earth Sciences 99, 1619-1632.
844 Sachau, T., Koehn, D. (2012) Melange: a viscoelastic lattice-particle model applicable to the
845 lithosphere. Geochemistry, Geophysics, Geosystems 13, 1-26.
846 Schenk, O., Urai, J. L., 2004. Microstructural evolution and grain boundary structure during
847 static recrystallization in synthetic polycrystals of sodium chloride containing saturated
848 brine. Contributions to Mineralogy and Petrology 146, 671–682.
849 Schenk, O., Urai, J.L. 2005. The migration of fluid-filled grain boundaries in recrystallizing
850 synthetic bischofite: first results of in-situ high-pressure, high-temperature deformation
851 experiments in transmitted light. J. Metamorph. Geol. 23, 695-709.
852 Schmid, S.M., Panozzo, R., Bauer, S., 1987. Simple shear experiments on calcite rocks:
853 rheology and microfabric. Journal of structural Geology 9, 747-778.
854 Seyfried, W.E., Foustoukos, D.I., Fu, Q., 2007. Redox evolution and mass transfer during
855 serpentinization: An experimental and theoretical study at 200° C, 500bar with
856 implications for ultramafic-hosted hydrothermal systems at Mid-Ocean
857 Ridges. Geochimica et Cosmochimica Acta 71, 3872-3886.

858 Smith, J.R., Piazolo, S., Daczko, N.R., Evans, L., 2015. The effect of pre- tectonic reaction
859 and annealing extent on behaviour during subsequent deformation: insights from paired
860 shear zones in the lower crust of Fiordland, New Zealand. Journal of Metamorphic
861 Geology 33, 557-577.
862 Spruzeniece, L., Piazolo, S., Maynard-Casely, H.E., 2017. Deformation-resembling
863 microstructure created by fluid-mediated dissolution-precipitation reactions, *Nature*
864 *Communications* 8.
865 Steinbach, F., Bons, P.D., Griera, A., Jansen, D., Llorens Verde, M.G., Roessiger, J.,
866 Weikusat, I., 2016. Strain localization and dynamic recrystallization in the ice–air
867 aggregate: a numerical study. The Cryosphere 10, 3071-3089.
868 Steinbach F., Kuiper, E-J. N., Eichler, J., Bons P.D., Drury M. R., Griera, A., Pennock, G.M.,
869 Weikusat I., 2017. The Relevance of Grain Dissection for Grain Size Reduction in Polar
870 Ice: Insights from Numerical Models and Ice Core Microstructure Analysis. Frontiers in
871 Earth Science 5, 66.
872 Stipp, M., Stünitz, H., Heilbronner, R., Schmid, S.M. 2002. The eastern Tonale fault zone: a
873 'natural laboratory' for crystal platic deformation of quartz over a temperature range from
874 250 to 750 °C. J. Struct. Geol. 24, 1861-1884.
875 Sundberg, M. & Cooper, R. F., 2008. Crystallographic preferred orientation produced by
876 diffusional creep of harzburgite: Effects of chemical interactions among phases during
877 plastic flow. Journal of Geophysical Research-Solid Earth 113.
878 ten Brink CE, Passchier CW. 1995. Modelling of mantle porphyroclasts using non-
879 Newtonian rock analogue materials. J Struct Geol 17, 131-146
880 Taylor GI. 1938. Plastic strain in metals. Journal of the Institute of Metals 62, 307–324.
881 Urai, J.L., 1983. Water assisted dynamic recrystallization and weakening in polycrystalline
882 bischofite. Tectonophysics 96, 125-157.

883 Urai, J. L., Humphreys, F. J., 1981. The development of shear zones in polycrystalline
884 camphor. Tectonophysics, 78, 677–685.
885 Urai, J. L., Humphreys, F. J., Burrows, S. E., 1980. In-situ studies of the deformation and
886 dynamic recrystallization of rhombohedral camphor. Journal of Materials Science 15,
887 1231–1240.
888 Urai, J. L., Means, W. D., Lister, G. S. 1986. Dynamic recrystallization of minerals. In:
889 Mineral and Rock Deformation: Laboratory Studies (edited by Hobbs, B. E. & Heard, H.
890 C.). Am. Geophys, Un. Geophys. Monogr. 36,161-199.
891 Vel, S.S., Cook, A., Johnson, S.E., Gerbi, C., 2016. Computational Homogenization and
892 Micromechanical Analysis of Textured Polycrystalline Materials, Computer Methods in
893 Applied Mechanics and Engineering 310, 749-779.
894 Vernon, R.H., 2004. A practical guide to rock microstructures. Cambridge University Press,
895 Cambridge.
896 Walte, N.P., Bons, P.D., Passchier, C.W. 2005. Deformation of melt-bearing systems -
897 insight from in situ grain-scale analogue experiments. Journal of Structural Geology 27,
898 1666-1679.
899 Wark, D.A., Watson, E.B., 2006. TitaniQ: a titanium-in-quartz geothermometer.
900 Contributions to Mineralogy and Petrology 152, 743-754.
901 Wheeler, J., 2009. The preservation of seismic anisotropy in the Earth's mantle during
902 diffusion creep. Geophysical Journal International 178, 1723-1732.
903 Wheeler, J., 2010. Anisotropic rheology during grain boundary diffusion creep and its
904 relation to grain rotation, grain boundary sliding and superplasticity. Philosophical
905 Magazine 90, 2841-2864.

Wheeler, J. 2014. Dramatic effects of stress on metamorphic reactions. Geology 42, 647-650.Wheeler, J., 2018. The effects of stress on reactions in the Earth: sometimes rather mean, usually normal, always important. Journal of Metamorphic Geology 36, 439-461.

Wilson, C. J. L. 1986. Deformation induced recrystallization of ice: the application of in situ experiments. Mineral and rock deformation: laboratory studies: The Paterson volume, 213-232.

Wilson, C. J., Peternell, M., Piazolo, S., Luzin, V. 2014. Microstructure and fabric development in ice: lessons learned from in situ experiments and implications for understanding rock evolution. Journal of Structural Geology 61, 50-77.

916 **Table Captions**

917 **Table 1** List of numerical models of microstructural (mm to dm) development identifying
918 processes modelled, numerical method used and providing relevant references. This list is
919 restricted to geological applications and those referenced in the main text. Note processes are
920 categorized as *"S"* for *static* (material points do not move) and *"D"* for *dynamic* (material
921 points move). Furthermore, unless stated otherwise models are two-dimensional.
922 Abbreviations: TBH – Taylor Bishop Hill calculation method for crystal lattice rotation,
923 VPFFT – Viscoplastic Fast Fourier Transform based model, EVPFFT - Elasto-viscoplastic
924 Fast Fourier Transform based model, FEM Finite Element, reXX – recrystallization.
925

926 **Figure Captions**

927 **Figure 1** Microstructural development during in-situ deformation of the rock analogue
928 octochloropropane within a circular shear zone (Bons and Jessell, 1999); dashed red lines
929 indicate the shear distribution between the two steps shown. Experiments run with top to the
930 right shear at an average strain rate of $4.6 \cdot 10^{-4}$ s^{-1} where the strain rate near edge of the shear
931 zone (~$1.2 \cdot 10^{-3}$ s^{-1}) is 10 x higher than in the top half of the image (~$1.2 \cdot 10^{-4}$ s^{-1}). (a) t_1 at a
932 bulk shear strain of ~40; (b) t_1+16 min.. Note multiple concurrent processes: grain boundary
933 migration, leading to dissection of grains (locations 1 & 2), subgrain rotation (black arrow),
934 nucleation (white arrow). The different shear rates lead to a different balance of
935 recrystallization processes and differences in microstructures. At the low shear rate grains are
936 equant, have straight sub-grain boundaries and basal planes at an angle to the NS and EW
937 polarisers. The high-strain rate zone shows serrate grain boundaries, an oblique grain-shape
938 foliation, basal grains approximately parallel to the shear-zone boundary, as well as shear
939 localisation on grain boundaries (location 3), indicative of grain boundary sliding/shearing.

940 Such "micro-shear zones" may now have been detected in polar ice sheets as well (Weikusat
941 et al., 2009).
942 **Figure 2** Numerical representation of a microstructure. (a) Micrograph of quartzite; (b)
943 numerical representation combining an element data structure with nodes (black circles),
944 segments (black lines) and polygons (enclosed area) and a lattice data structure with
945 unconnected lattice points (open circles). This structure is used in the numerical platform Elle
946 (see text for details).
947 **Figure 3** Numerical modelling of dynamic recrystallization – a historical perspective;
948 mineral modelled is quartz; simple shear (see text for details); (a) numerical microstructure
949 after γ= 1; different grey scales signify different crystallographic orientations; top inset shows
950 data structure of hexagonal lattice points (modified after Jessell and Lister, 1990); (b)
951 numerical microstructure after γ= 1; colours show crystallographic orientation, grain
952 boundaries are red, subgrain boundaries black; for data structure see inset (modified after
953 Piazolo et al., 2002).
954 **Figure 4** Numerical modelling of dynamic recrystallization – testing the effect of process
955 combination on microstructural development; model parameters: mineral modelled - ice; time
956 step - 20 years, simple shear; $\Delta\gamma$ - 0.04 per time step. FFT and GBM signify fast fourier
957 transform formulation for crystal plasticity and grain boundary migration, respectively; (a)
958 initial microstructure and results after γ=2.4 for different process combinations. Results are
959 shown as grain network with orientation related colour coding according to crystal
960 orientations relative to the shortening direction y (see legend) and in pole figures. In the latter
961 the colour bar indicates the multiples of uniform distribution; (b) grain area distribution
962 normalized to the initial average grain area for all models shown.
963 **Figure 5** Results from diffusion creep modelling in pure shear; 2D microstructure as in the
964 starting frame of Fig 1b of Wheeler (2009). Shown is the oblique view of microstructure with

patterns of normal stress shown along grain boundaries in the 3rd dimension as "fences". Red arrows show stretching direction, hence stresses are tensile (shown as negative) on boundaries at a high angle to stretching direction are tensile. Fences are colour coded according to dissolution rate with blue low and red high. When there is no relative grain rotation the fences have a single colour and the stress is parabolic. When there is relative grain rotation the fences vary in colour and the stress is a cubic function of position.

Figure 6 Dynamic development of stylolite roughness in numerical simulations; (a) time series (left to right) with the stylolite nucleating in the middle of a slow dissolving layer (layer in green and stylolite in black colour). Once the stylolite has dissolve the layer on one side the layer starts to pin and teeth develop. (b) Variation of the pinning strength of the layer in three different simulations showing a strong dependency. The compaction (movement of upper and lower walls) is shown in quite arrows. L in the picture on the right hand side is the initial position of the layer and P shown as black arrows indicates the pinning of the layer upwards and downwards during dissolution.

Figure 7 Example of new development in microdynamic numerical modelling; preliminary results (see text for details). (a) Coupling of diffusion creep and surface energy driven grain boundary migration (GBM); (left) starting microstructure; (middle) microstructure at stretch 2; (right) graph showing average aspect ratio versus stretch; note that the microstructure after a significant period of exclusive grain boundary migration is the same as the starting microstructure as no movement occurs as all triple junctions are 120°. Number of grains stays constant for all simulations. (b) Evolution of chemical concentration of an arbitrary element during surface energy driven GBM. The material is a single-phase polycrystalline aggregate with different initial chemical content. This example assumes very low bulk diffusion (D_{bulk} =1e^{-20} m^2/s) and fast grain boundary diffusion ($D_{boundary}$ =1e^{-8} m^2/s), hence grain boundary diffusion dominates. Colour code indicates chemical concentration and white

990 lines represent grain boundaries. (c) Dissolution of reactive surfaces in 3D using the example
991 of fluorite dissolution. Microstructures after three dissolution periods are show (150hrs, 180
992 hrs, 276 hrs); surfaces correspond to the {111} plane at the start of experiment/simulation;
993 colours identify different depths where blue signifies low and red high; images are 60 μm
994 width. Top panel row shows numerical results. Lower panel shows experimental results using
995 confocal microscopy images of a grain of a sintered CaF_2 pellet at the same three dissolution
996 times as the numerical models. Note the formation of etch pits with similar triangular shape
997 and the faster/enhanced dissolution of the grain boundaries in both experiment and numerical
998 simulations.

Figure1

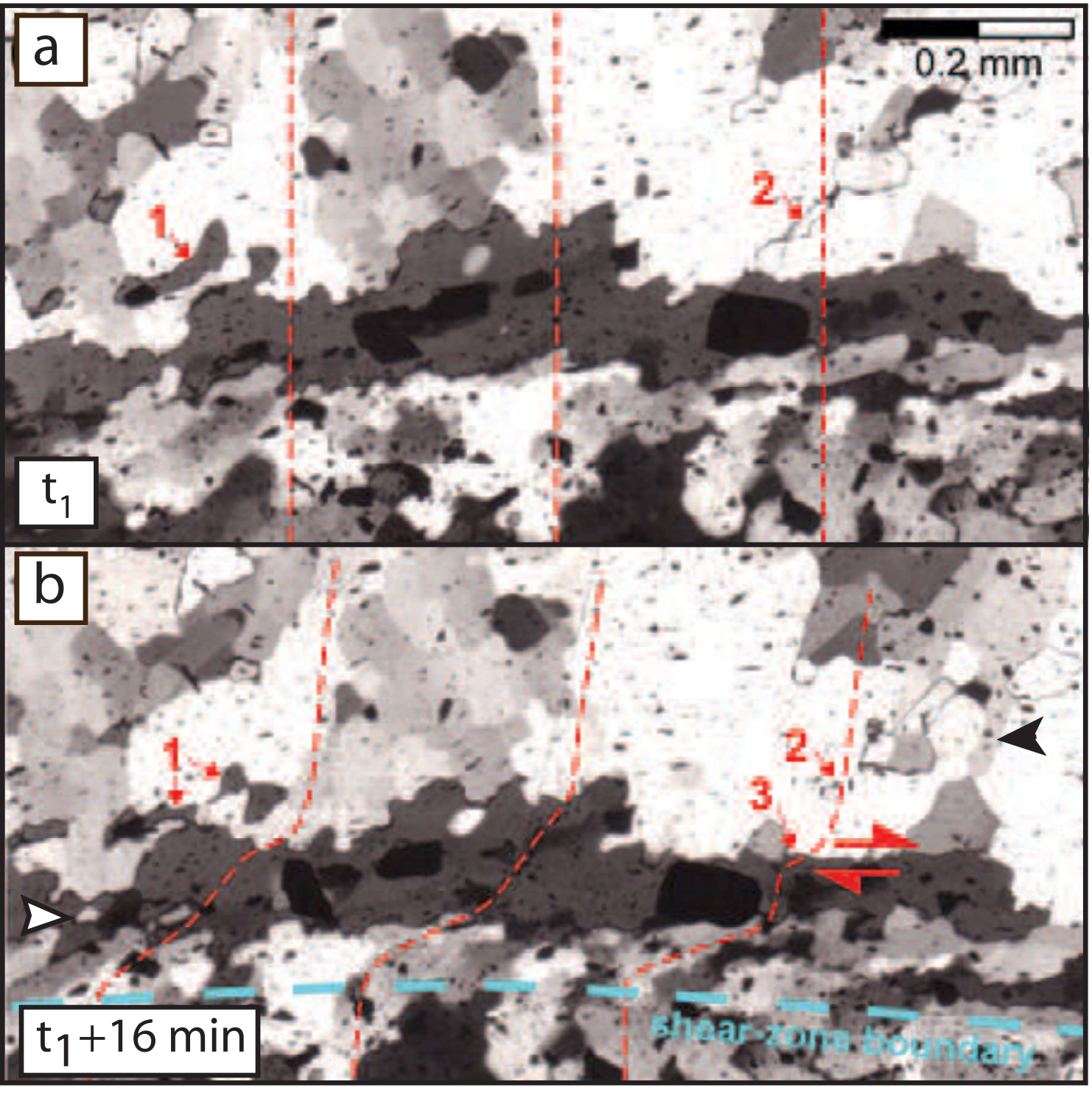
a
0.2 mm
1
2
t1
b
1
2
3
t1+16 min
shear-zone boundary
strain rate increase

Figure 2

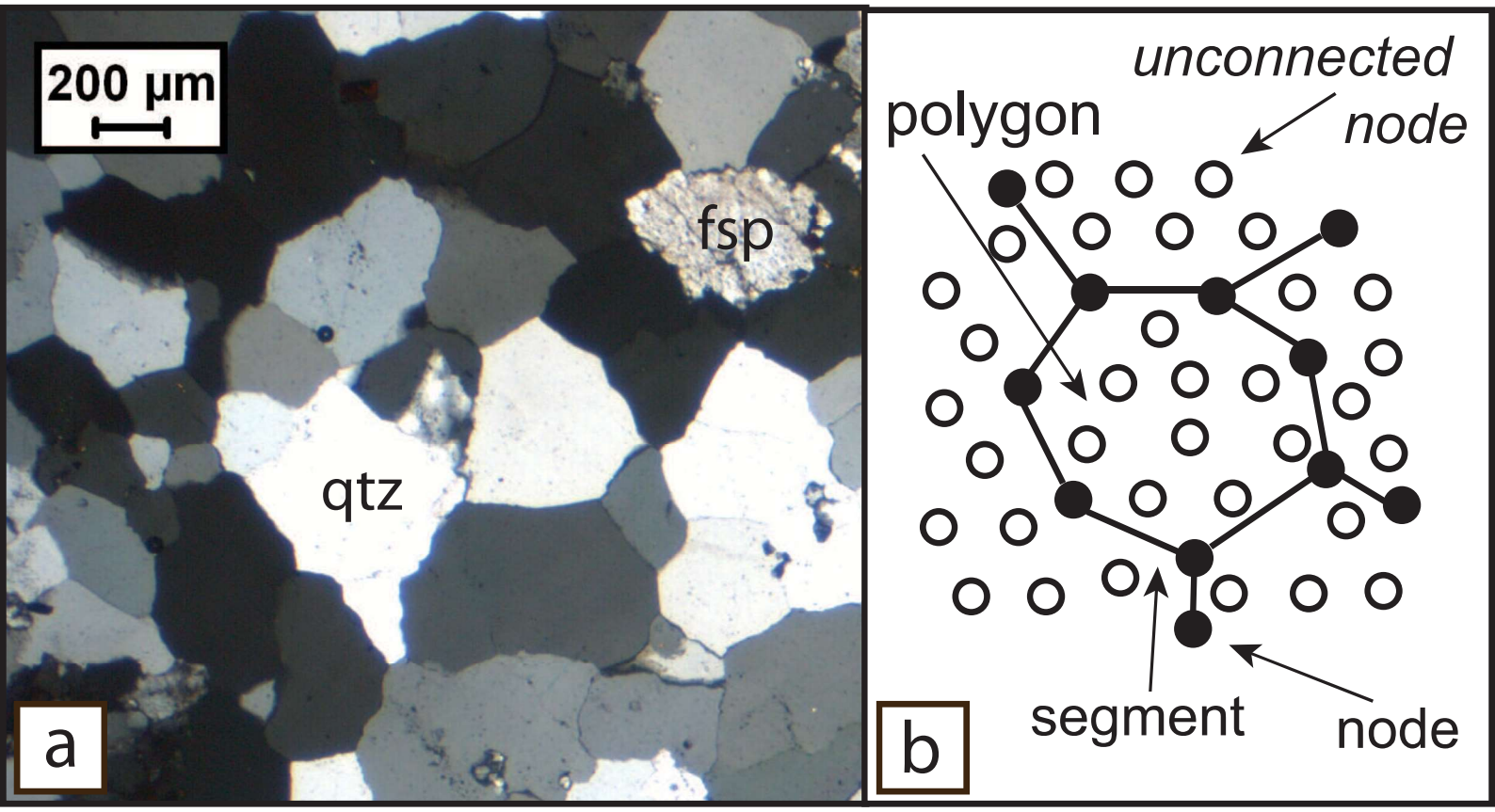

Figure 3

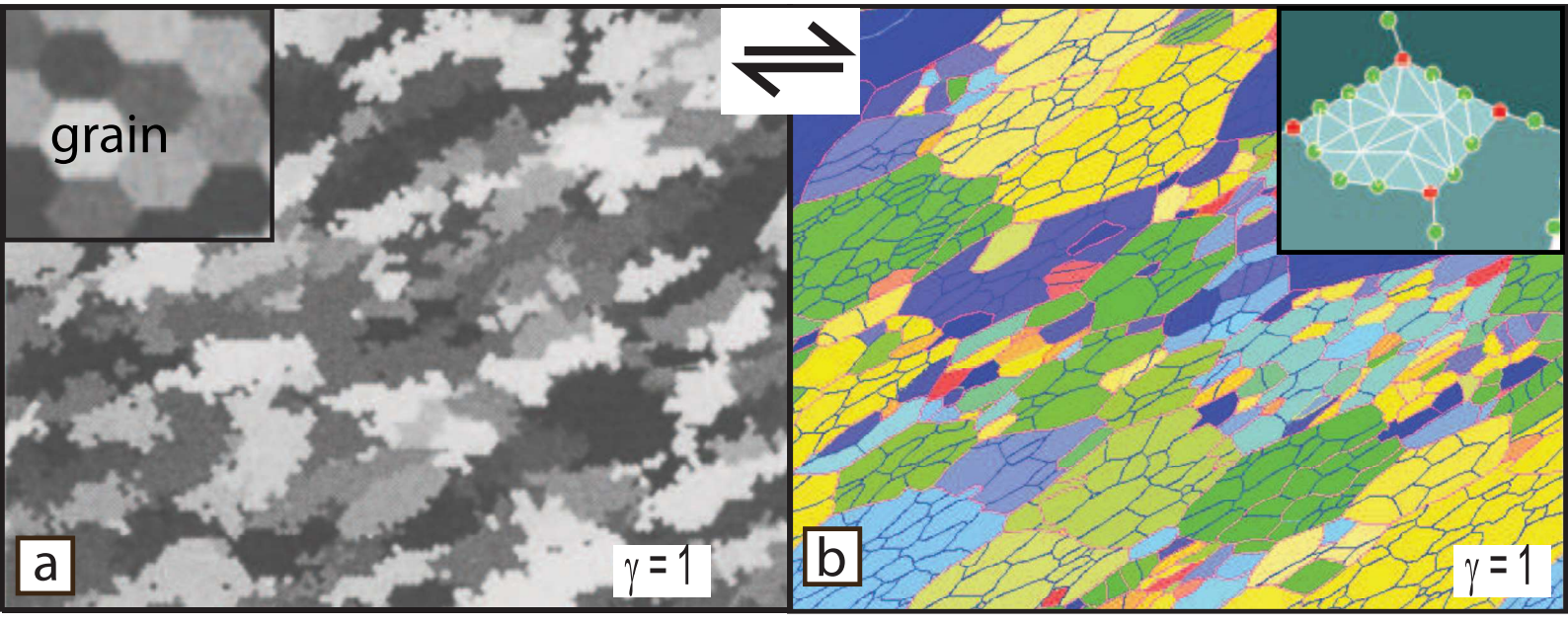

Figure 4

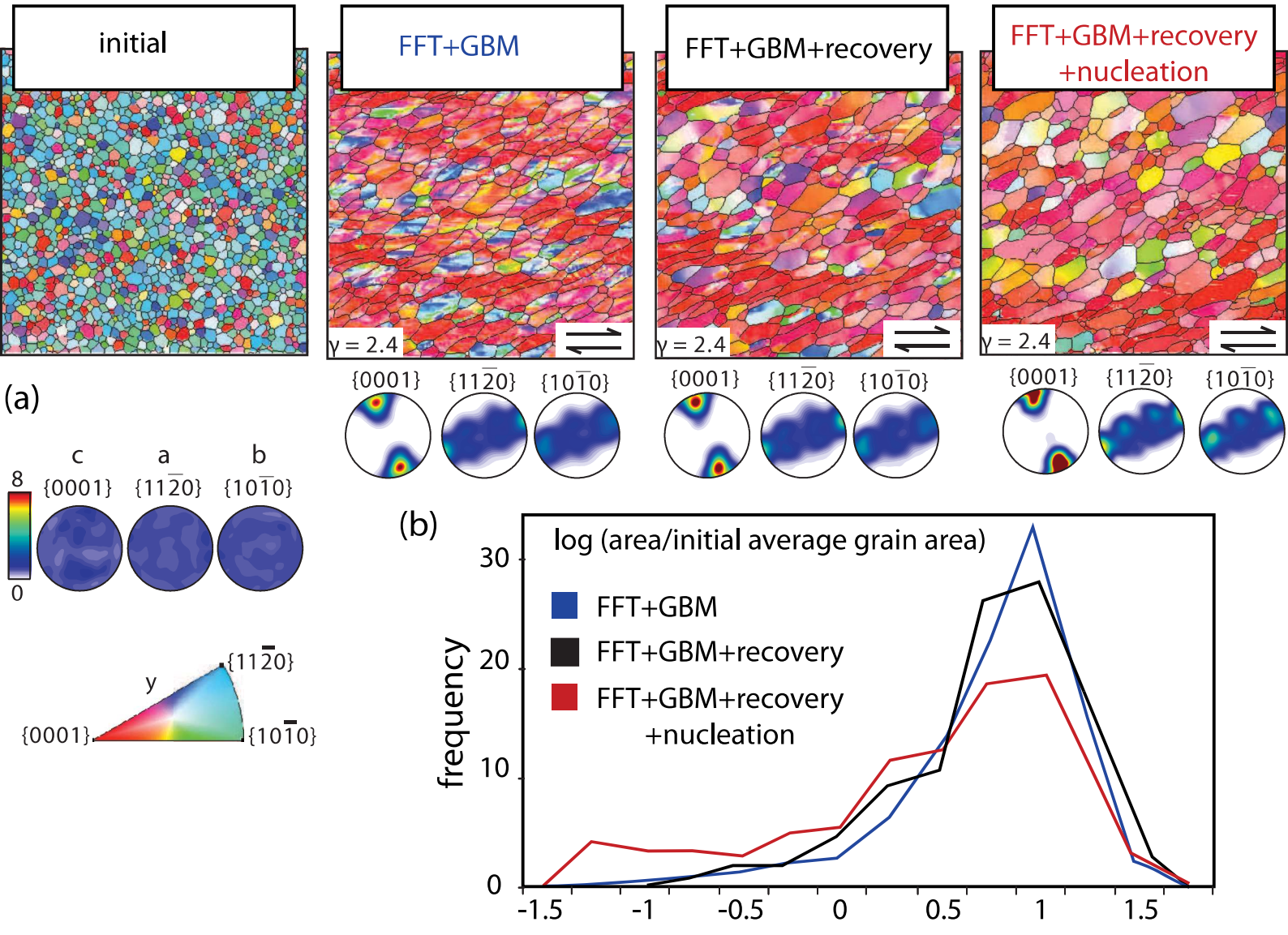
initial
FFT+GBM
FFT+GBM+recovery
FFT+GBM+recovery
+nucleation
γ = 2.4
γ = 2.4
γ = 2.4
{0001}
{11$\bar{2}$0}
{10$\bar{1}$0}
{0001}
{11$\bar{2}$0}
{10$\bar{1}$0}
{0001}
{11$\bar{2}$0}
{10$\bar{1}$0}
(a)
c
a
b
{0001}
{11$\bar{2}$0}
{10$\bar{1}$0}
8
0
y
{11$\bar{2}$0}
{0001}
{10$\bar{1}$0}
(b)
log (area/initial average grain area)
FFT+GBM
FFT+GBM+recovery
FFT+GBM+recovery
+nucleation
frequency
30
20
10
0
-1.5
-1
-0.5
0
0.5
1
1.5

Figure 5

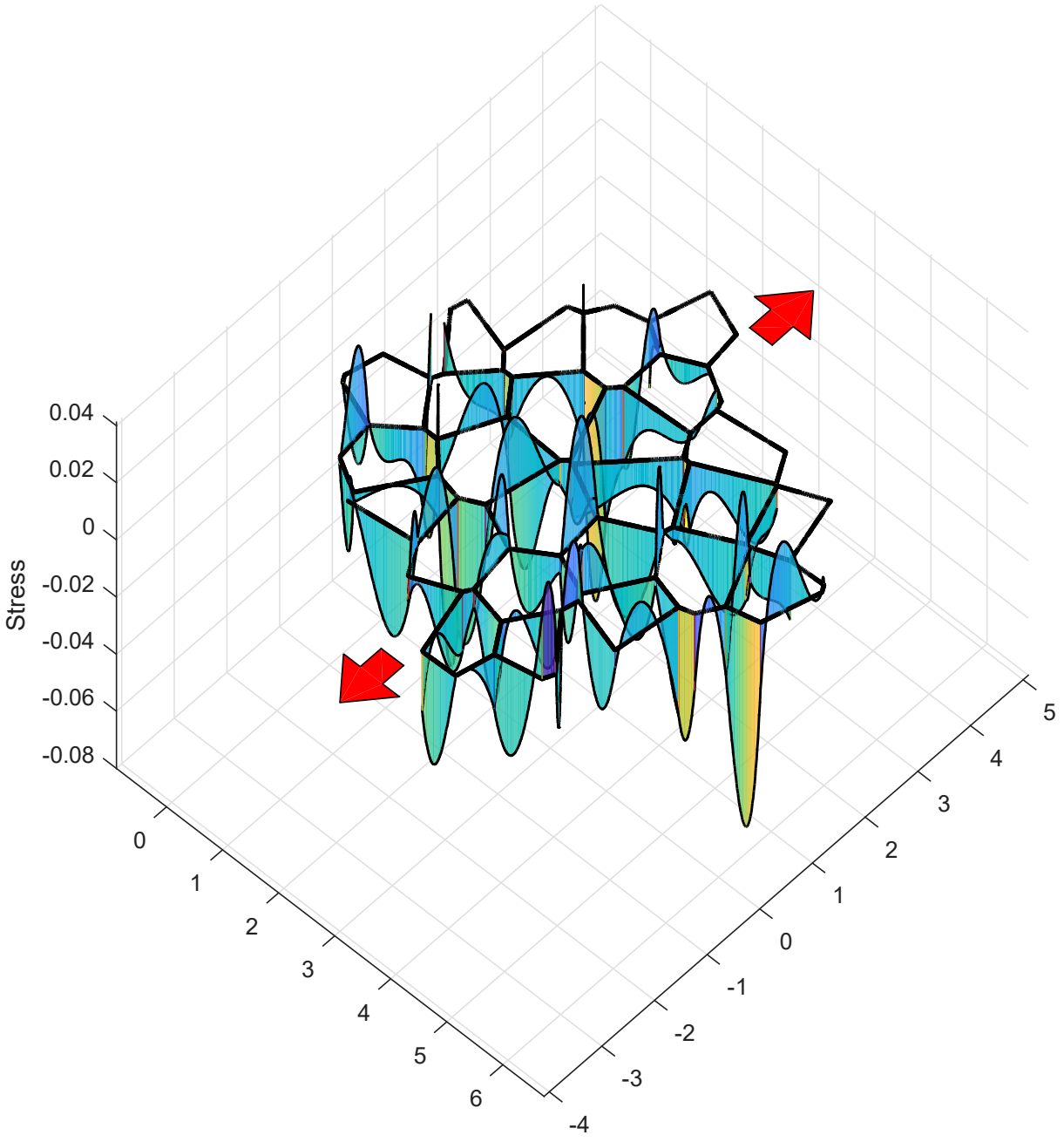

Figure 6

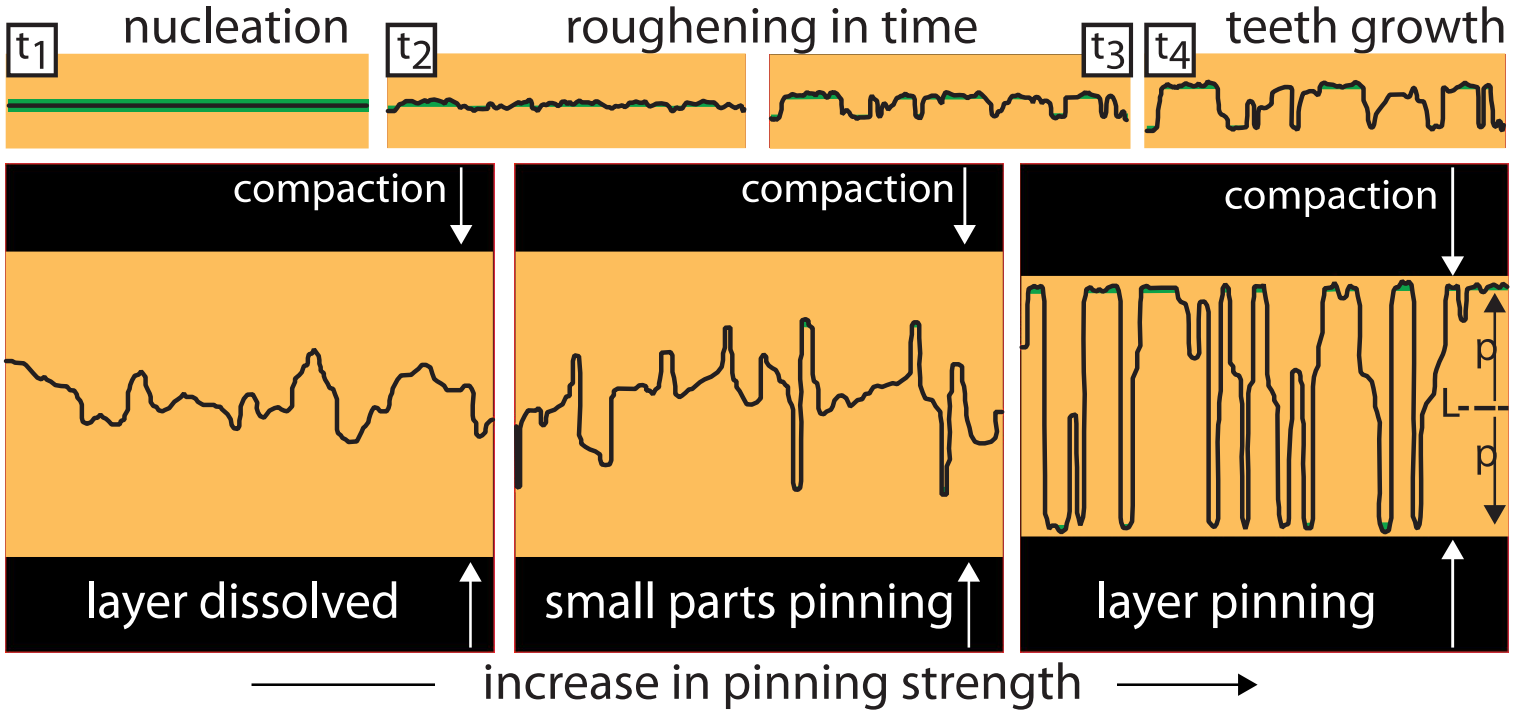
t1
nucleation
t2
roughening in time
t3
t4
teeth growth
compaction
compaction
compaction
p
L
p
layer dissolved
small parts pinning
layer pinning
increase in pinning strength

Figure 7

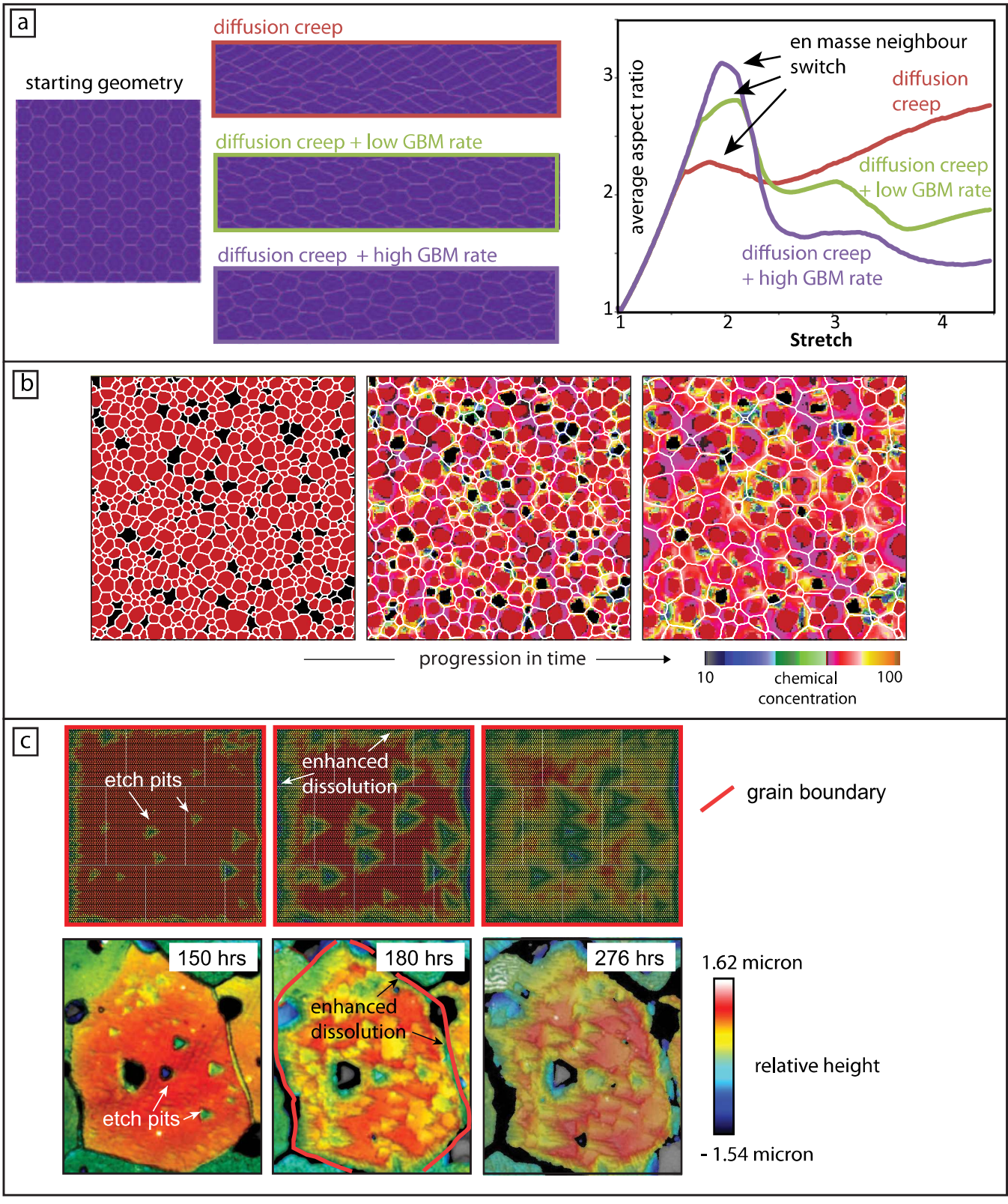
a
starting geometry
diffusion creep
diffusion creep + low GBM rate
diffusion creep + high GBM rate
en masse neighbour switch
diffusion creep
diffusion creep + low GBM rate
diffusion creep + high GBM rate
average aspect ratio
Stretch
b
progression in time
10
chemical concentration
100
c
etch pits
enhanced dissolution
grain boundary
150 hrs
180 hrs
276 hrs
etch pits
enhanced dissolution
1.62 micron
relative height
- 1.54 micron

Table 1

(micro) structure/process		Numerical Method	References
General papers – review, overview, state of the art			Jessell et al., 2001; Jessell and Bons, 2002; Bons et al., 2008; Piazolo et al., 2010
Single processes			
Crystal lattice rotation for single phase	*D*	slip, rotation, translation	Etchecopar, 1977
	D	TBH	Lister and Paterson, 1979
	D	VPFFT	Lebensohn et al., 2001; Montagnat et al. ,2011, 2014
	D	VPFFT – 3D	Roters et al., 2012; Eisenlohr et al., 2013
Grain rotations for two phases	*D*	VPFFT	Griera et al., 2011, 2013, 2015; Ran et al., 2018
Elasto-viscoplastic behaviour	*D*	EVPFFT	Lebensohn et al., 2012
	D	lattice spring model + viscous deformation	Sachau and Koehn, 2010, 2012; Arslan et al., 2012; Koehn and Sachau, 2014
Diffusion creep for single phase	*D*	front tracking	Ford et al., 2002, 2004; Wheeler, 2009, 2010
Diffusion creep for two phases	*D*	front tracking	Berton et al., 2006, 2011; Ford and Wheeler, 2004
Dissolution and/or precipitation	*D*	lattice spring model	Koehn et al., 2006, 2007, 2012, 2016; Ebner et al., 2009,
Dissolution at reactive surfaces	*D*	front tracking	Godinho et al., 2014
		front tracking - 3D	Piazolo et al. *this contribution*
Grain growth			
– isotropic surface energy	*S*	front tracking	Roessiger et al. 2011, 2014
– isotropic surface energy	*SD*	front tracking (triple points only)	Bons & Urai, 1992
– anisotropic surface energy	*S*	front tracking	Becker et al., 2008; Piazolo et al., 2016
– growth with pinning	*S*	front tracking	Kelka et al., 2015
– isotropic grain growth	*SD*	Potts – 2 & 3D	Kim et al. 2006; Krill and Chen, 2002
– two phases	*S*	front tracking	Roessiger et al., 2014
Growth of crystals into a crack or in strain fringes	*SD*	phase field – 3D	Ankit et al., 2015
	D	front tracking	Hilgers et al. ,1997; Koehn et al., 2003
Strain-induced grain boundary migration	*S*	front tracking	Becker et al., 2008; Roessiger et al., 2011
Single phase ductile deformation without reXX + crystallography	*D*	FEM – thin sheet model	Barr and Houseman, 1992, 1996
Grain boundary diffusion	*S*	finite difference	Park et al., 2004
Strain/stress localisation	*D*	VPFFT	Griera et al., 2011, 2015; Ran et al., 2018
Combination of Processes			
Intracrystalline recovery and subgrain rotation	*S*	Potts-like	Borthwick et al., 2013
Ductile deformation and grain growth - polyphase	*D*	FEM + front tracking	Groome et al., 2006; Smith et al., 2015
Dynamic reXX:	*D*	TBH+Potts-like	Jessell, 1988a, b; Jessell & Lister, 1990
- crystal plastic deformation, grain boundary migration, rotation recrystallization			
- grain growth and polygonisation	*S*	front tracking	Roessiger et al., 2011
- crystal plastic deformation, grain boundary migration, rotational recrystallization, nucleation, recovery	*D*	TBH+FEM+front tracking	Piazolo et al., 2002
- crystal plastic deformation, grain boundary migration, rotational recrystallization, recovery	*D*	VPFFT+ front tracking	Jansen et al., 2016; Llorens et al., 2016a, b, 2017; Steinbach et al., 2016, 2017; Gomez-Rivas et al., 2017; Piazolo et al., *this contribution*
Strain/stress localization	*D*	FEM+front tracking	Jessell et al., 2005; Gardner et al., 2017
- linked to grain size variations & rheology			
- linked to grain size variations & rheology	*D*	FEM	Cross et al., 2015
Diffusion and grain growth	*D*	front tracking	Piazolo et al. *this contribution*
Trace element diffusion and reXX	*S*	front tracking	Piazolo et al. *this contribution*